Article

Cell Reports

ROCK-Isoform-Specific Polarization of Macrophages Associated with Age-Related Macular Degeneration

Graphical Abstract

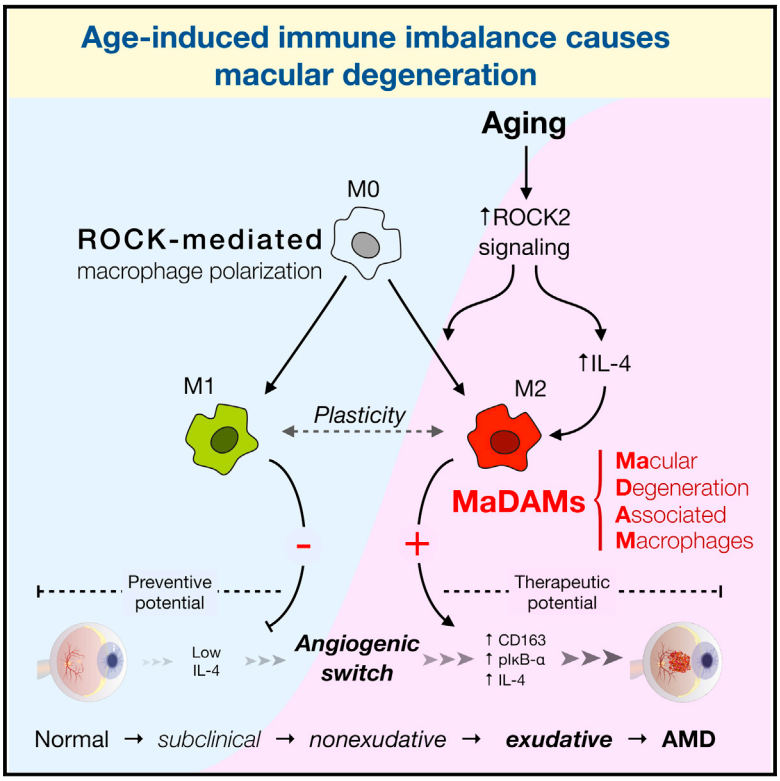

Highlights

- ROCK isoforms determine macrophage polarization
- M2-like macrophages are critical in age-related macular degeneration (AMD)
- Age-induced macrophage polarization explains the angiogenic switch in exudative AMD
- Targeting ROCK2 restores the normal macrophage balance found in the young eye

Authors

Souska Zandi, Shintaro Nakao, ..., Tatsuro Ishibashi, Ali Hafezi-Moghadam

Correspondence

ahm@bwh.harvard.edu

In Brief

How age is linked to age-related macular degeneration (AMD) is unknown. Zandi et al. now describe altered ROCK signaling and macrophage polarization in the aging eye. The ensuing imbalance toward M2 macrophages explains the angiogenic switch in AMD. Selective ROCK2 inhibition restores the balanced condition found in the young eye.

Zandi et al., 2015, Cell Reports *10*, 1173–1186
February 24, 2015
http://dx.doi.org/10.1016/j.celrep.2015.01.050

CellPress

Cell Reports
Article

ROCK-Isoform-Specific Polarization of Macrophages Associated with Age-Related Macular Degeneration

Souska Zandi,[1,2,3,4,5,17] Shintaro Nakao,[1,2,3,4,6,17] Kwang-Hoon Chun,[7] Paolo Fiorina,[8,9] Dawei Sun,[1,2,3,4,10] Ryoichi Arita,[6] Ming Zhao,[1,2,11] Enoch Kim,[12] Olivier Schueller,[12] Stewart Campbell,[12] Mahdi Taher,[1,2,3,4] Mark Ivan Melhorn,[1,2,3,4] Alexander Schering,[1,2,3,4] Francesca Gatti,[8,9] Sara Tezza,[8,9] Fang Xie,[1,2,3,4,10] Andrea Vergani,[8,9] Shigeo Yoshida,[6] Keijiro Ishikawa,[6] Muneo Yamaguchi,[6] Fumiyuki Sasaki,[13] Ruth Schmidt-Ullrich,[14] Yasuaki Hata,[6] Hiroshi Enaida,[6] Mitsuko Yuzawa,[15] Takehiko Yokomizo,[13] Young-Bum Kim,[16] Paul Sweetnam,[12] Tatsuro Ishibashi,[6] and Ali Hafezi-Moghadam[1,2,3,4,*]

[1]Center for Excellence in Functional and Molecular Imaging, Brigham & Women's Hospital, Boston, MA 02115, USA
[2]Department of Radiology, Harvard Medical School, Boston, MA 02115, USA
[3]Angiogenesis Laboratory, Massachusetts Eye & Ear Infirmary, Boston, MA 02114, USA
[4]Department of Ophthalmology, Harvard Medical School, Boston, MA 02115, USA
[5]Department of Ophthalmology, Swiss Eye Institute, Rotkreuz and Berner Augenklinik am Lindenhofspital, 3012 Bern, Switzerland
[6]Department of Ophthalmology, Graduate School of Medical Sciences, Kyushu University, Fukuoka 812-8582, Japan
[7]Gachon Institute of Pharmaceutical Sciences, College of Pharmacy, Gachon University, Incheon 406-799, Republic of Korea
[8]Nephrology Division, Boston Children's Hospital, Harvard Medical School, Boston, MA 02115, USA
[9]Division of Transplant Medicine, San Raffaele Hospital, 20132 Milan, Italy
[10]Department of Ophthalmology, the First and Second Affiliated Hospitals of the Harbin Medical University, Harbin 150086, China
[11]State Key Laboratory of Oncology, Minimally Invasive Interventional Division, Medical Imaging Center, Sun Yat-Sen University, Guangzhou 510060, China
[12]Surface Logix, Inc., 50 Soldiers Field Place, Brighton, MA 02135, USA
[13]Department of Biochemistry, Juntendo University School of Medicine, Tokyo 113-8421, Japan
[14]Department of Signal Transduction in Tumor Cells, Max-Delbrück-Center for Molecular Medicine, Robert-Rössle-Straße 10, 13092 Berlin, Germany
[15]Department of Ophthalmology, School of Medical Sciences, Nihon University, Tokyo 173-8610, Japan
[16]Division of Endocrinology, Diabetes and Metabolism, Beth Israel Deaconess Medical Center and Harvard Medical School, Boston, MA 02115, USA
[17]Co-first author
*Correspondence: ahm@bwh.harvard.edu
http://dx.doi.org/10.1016/j.celrep.2015.01.050

SUMMARY

Age is a major risk factor in age-related macular degeneration (AMD), but the underlying cause is unknown. We find increased Rho-associated kinase (ROCK) signaling and M2 characteristics in eyes of aged mice, revealing immune changes in aging. ROCK isoforms determine macrophage polarization into M1 and M2 subtypes. M2-like macrophages accumulated in AMD, but not in normal eyes, suggesting that these macrophages may be linked to macular degeneration. M2 macrophages injected into the mouse eye exacerbated choroidal neovascular lesions, while M1 macrophages ameliorated them, supporting a causal role for macrophage subtypes in AMD. Selective ROCK2 inhibition with a small molecule decreased M2-like macrophages and choroidal neovascularization. ROCK2 inhibition upregulated M1 markers without affecting macrophage recruitment, underlining the plasticity of these macrophages. These results reveal age-induced innate immune imbalance as underlying AMD pathogenesis. Targeting macrophage plasticity opens up new possibilities for more effective AMD treatment.

INTRODUCTION

Age-related macular degeneration (AMD) is the leading cause of adult vision loss in the developed countries. AMD has two types, the dry form that ultimately leads to macular atrophy and the more rapidly progressing wet form, characterized by choroidal neovascularization (CNV) and leakage. Most AMD cases are of the dry atrophy type, which can become exudative due to CNV. The normal choroid maintains quiescence through an excess of antiangiogenic versus proangiogenic factors. Little is known about what might reverse that balance and lead to an angiogenic switch. While aging is the strongest risk factor for AMD (Klein et al., 2002), how age influences pathogenesis is unknown. Current drug therapy in AMD is based on repeated intravitreal injections of vascular endothelial growth factor A (VEGF-A) inhibitors, which only

reduce symptoms. A recent study showed macular atrophy in virtually all long-term anti-VEGF-A-treated AMD cases, one third of which suffered alarming visual decay (Rofagha et al., 2013).

Macrophages are found in AMD lesions (Tsutsumi et al., 2003); however, their detailed role in the disease is not understood. Plasticity and diversity are fundamental characteristics of macrophages (Sica and Mantovani, 2012). Undifferentiated M0 macrophages can polarize into classical proinflammatory M1-like and alternative anti-inflammatory M2-like macrophages, two extremes in a continuum of polarization states (Sica and Mantovani, 2012). A mixture of polarization phenotypes coexist, which reflect the highly dynamic and complex tissue conditions. Furthermore, polarized macrophages show a high level of plasticity in response to tissue signals. Therefore, elucidation of the mechanisms and molecules involved in macrophage polarization and plasticity may provide therapeutic avenues. Both M1- and M2-like subtypes are found in AMD (Cao et al., 2011); however, their roles in the pathogenesis have not been studied. Interleukin-1β (IL-1β), IL-12, IL-23, interferon-γ (IFN), lipopolysaccharine (LPS), and tumor necrosis factor-α (TNF-α) induce the M1-like phenotype that expresses CCL3, CCL5, CD80, CCR7, and inducible nitric oxide synthase (iNOS). In contrast, IL-4, IL-10, IL-13, and TGF-β promote the M2-like phenotype that expresses CCL22, CD206, CD163, Ym 1, Fizz 1, and arginase 1 (Mantovani et al., 2004).

Rho-associated, coiled-coil-containing protein kinases (ROCKs) are involved in cytoskeletal rearrangement, contractility (Riento and Ridley, 2003), angiogenesis, and inflammation (Arita et al., 2009). RhoA and RhoE are upstream of ROCK, which has two isoforms, ROCK1 and ROCK2, whose intracellular localizations differ depending on the type and condition of the examined cells (Chun et al., 2012). The role of ROCK isoforms in macrophage polarization and AMD is completely unexplored. ROCK substrates include myosin light chain (MLC), myosin binding subunit of myosin phosphatase (MYPT), and ezrin/radixin/moesin (ERM) proteins, while downstream targets include inhibitor of kappaB alpha (IκB-α) and nuclear factor-κB (NF-κB) (Cammarano and Minden, 2001).

Here we uncover a molecular switch for macrophage polarization through the ROCK signaling pathway. We show an M2-type shift with aging and establish the causal role of M2-like macrophages in CNV pathology.

RESULTS

Choroidal Neovascular Endothelium Expresses ROCK

To determine whether ROCK1 and ROCK2 are expressed in human AMD, surgically excised CNV membranes from AMD patients were used for immunohistochemistry. In these samples, we stained for both ROCK isoforms and for the von Willebrand Factor (vWF). Surgically excised CNV membranes from human AMD (n = 7) and idiopathic macular degeneration (n = 7) patients expressed high levels of both ROCK1 and ROCK2. In contrast, the retinal specimens from normal patients showed significantly less staining for either isoform (n = 5). Analogously, in the laser-induced CNV in mouse and monkey, ROCK1 and ROCK2 co-localized in angiogenic endothelium, but were expressed far less in normal vessels (Figure 1).

Increased ROCK Signaling in Choroidal Neovascularization

To investigate ROCK signaling in CNV, we performed western blots for ROCK isoforms and its substrate, MYPT1, in laser-induced CNV tissues in mice. MYPT1 phosphorylation peaked at 3 and 7 days following laser injury in the mouse choroid, while ROCK1 and ROCK2 expressions remained unchanged throughout the course of CNV. To block ROCK2 activity, we used a novel selective inhibitor (Figures S1 and S2). Dual ROCK1/2 and selective ROCK2 inhibition reduced pMYPT1 to normal unlasered levels (Figure 2A).

MLC phosphorylation was increased in CNV and reduced to normal levels with dual ROCK1/2 and selective ROCK2 inhibition. Upstream of ROCK, RhoA was significantly increased in CNV, while RhoE was unchanged. Dual ROCK1/2 and selective ROCK2 inhibition reduced RhoA expression in lasered eyes to those found in unlasered controls (Figure 2B). This could suggest a feedback loop for ROCK activity in regulating RhoA.

ROCK2 Inhibition Reduces Choroidal Neovascularization and Leakage

To investigate the role of ROCK in CNV, we induced CNV by laser injury and treated the mice with the dual ROCK1/2 inhibitor, fasudil, or the selective ROCK2 inhibitor and quantified lesion size and vascular leakage. CNV lesions were ~60% smaller with dual ROCK1/2 inhibition compared with control. Selective ROCK2 inhibition significantly reduced CNV in a dose-dependent fashion, 66% reduction at 1 mg/kg, while maximum efficacy was reached at 10 mg/kg. In comparison, the CNV size in ROCK1+/−Tie1Cre mice that have reduced endothelial ROCK1, did not differ from that of lasered Tie1Cre or WT control (Figure 2C).

Dual ROCK1/2 and selective ROCK2 inhibition suppressed the percentage of the clinically relevant grade IV leakage (Figure 2D). In comparison, ROCK1+/−TieCre showed the same amount of leakage as lasered WT mice (Figure 2E). Furthermore, intravitreal injections of fasudil in monkeys significantly reduced the percentage of grade IV leakages, as well as CNV membrane thickness (Figure 2F).

Endothelial NF-κB Not Required for CNV Formation

To study downstream mediators of ROCK, we measured IκB-α and pIκB-α in the eyes of normal and lasered mice with and without inhibitor treatments. IκB-α phosphorylation peaked 3 days after laser injury, while higher levels of NF-κB and phosphorylated NF-κB p65 (RelA) were detected by day 3 through 14 (Figure 3A). NF-κB protein expression was higher in CNV, possibly due to leukocyte accumulation. Dual ROCK1/2 and selective ROCK2 inhibition reduced CNV-induced NF-κB protein expression, as well as IκB-α and NFκB phosphorylations to levels found in unlasered eyes. The IκB-α protein expression was not affected by laser injury or the various treatments (Figure 3B). While our results are in line with the fact that IκB-α is downstream of ROCK, IκB-α can also be phosphorylated by other kinases.

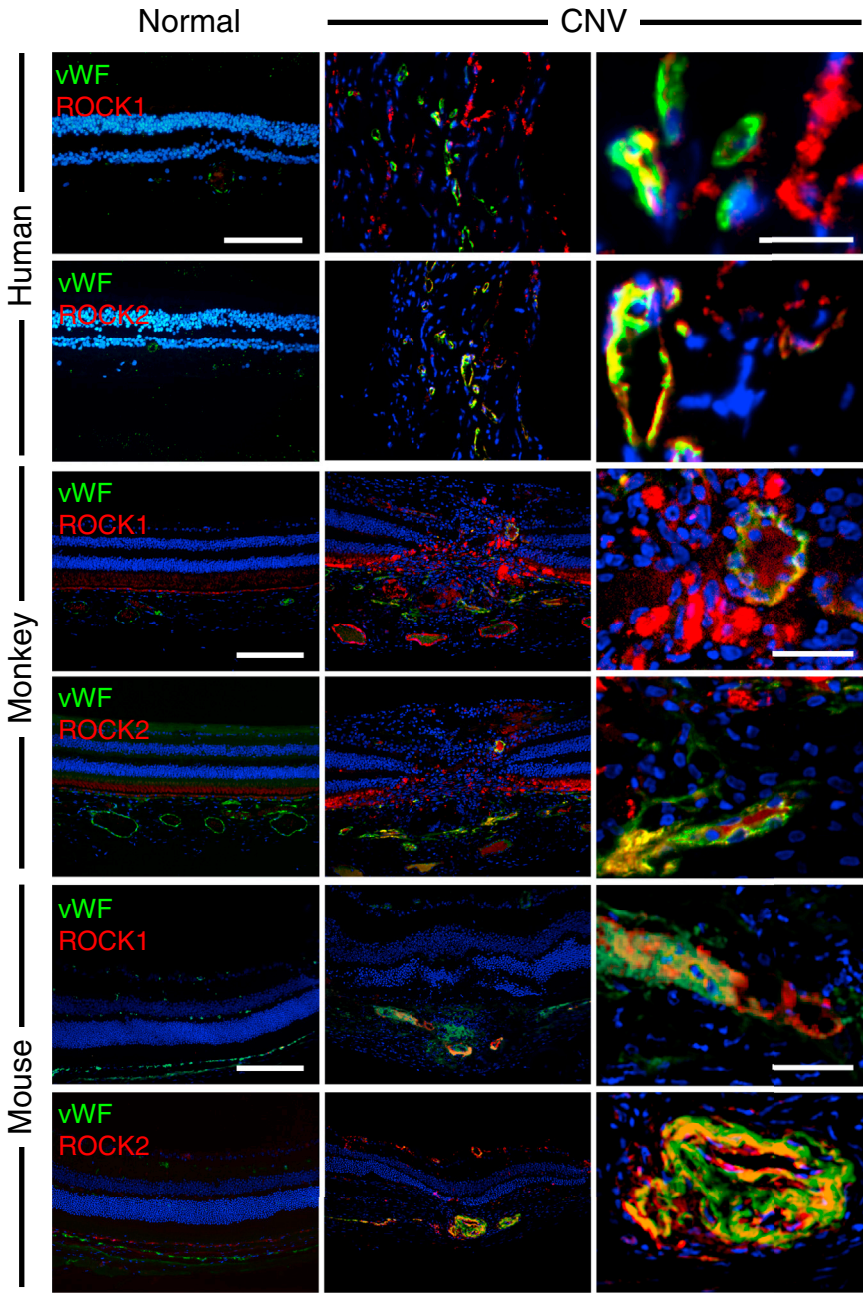

Figure 1. CNV Lesions Express Both ROCK Isoforms

Double immunostaining shows localizations of vWF (green) and ROCK1 or ROCK2 (red) in ocular tissues from normal retina-choroidal complexes and human AMD membranes, laser-induced CNV in monkey and in mice. In the CNV tissues of all three species, nonendothelial cells also expressed ROCK isoforms. Blue indicates nuclei stained with 4,6-diamidino-2-phenylindole (DAPI). The scale bar represents low magnification at 100 μm and high magnification at 20 μm.

NF-κB contributes to angiogenesis (Tabruyn and Griffioen, 2008), but its role in CNV is not understood. In the Tie1ΔN mouse, which lacks endothelial NF-κB signaling (Henke et al., 2007), CNV and leakage were the same as that in lasered WT or in the Tie1Cre control mice. However, ROCK2 inhibition in the Tie1ΔN mice significantly reduced CNV (Figures 3C and 3D).

ROCK Mediated Macrophage Infiltration in Choroidal Neovascularization

Macrophage recruitment in mice peaks 3 days after laser injury (Tsutsumi et al., 2003). The number of accumulated F4/80(+) macrophages in WT mice at day 3 was significantly reduced by dual ROCK1/2, but not by selective ROCK2 inhibition (Figure 4A). Lasered CD18−/− mice showed levels of F4/80(+) cells comparable to that of unlasered WT mice, indicating that the increased accumulation is due to recruitment.

In laser-induced CNV in monkey eyes, intravitreal fasudil injection significantly reduced macrophage infiltration (Figure 4B). Immunohistochemistry showed staining for both ROCK1 and ROCK2 isoforms in infiltrated macrophages in the CNV lesions of mouse and monkey, but not in normal control eyes (Figure 4C).

To investigate the differential impacts of dual ROCK1/2 versus ROCK2 inhibition on leukocyte transmigration from angiogenic vessels, we developed a new imaging technique (Figure S3). The combination of growth-factor-induced corneal angiogenesis with in vivo acridine orange (AO) labeling of leukocytes allowed visualization of leukocyte extravasation from normal and angiogenic vessels in a chemotactic gradient. In MCP-1 implanted corneas, dual ROCK1/2 inhibition suppressed leukocyte transmigration, while selective ROCK2 inhibition did not (Figure 4D). This is supported by our finding that dual ROCK1/2 inhibition or ROCK1 knockdown affects cytoskeletal proteins, while selective ROCK2 inhibition or ROCK2 knockdown does not (Figure S4).

ROCK Mediated Macrophage Polarization in Choroidal Neovascularization

The role of ROCK isoforms in macrophage polarization has previously not been investigated. In surgically excised membranes from AMD patients, ROCK1 and ROCK2 co-localized with CD206, expressed on M2 macrophages (Figure 5A). CD80(+) cells expressed ROCK1 and ROCK2 in neovascular tissues from AMD patients, whereas normal eyes did not stain

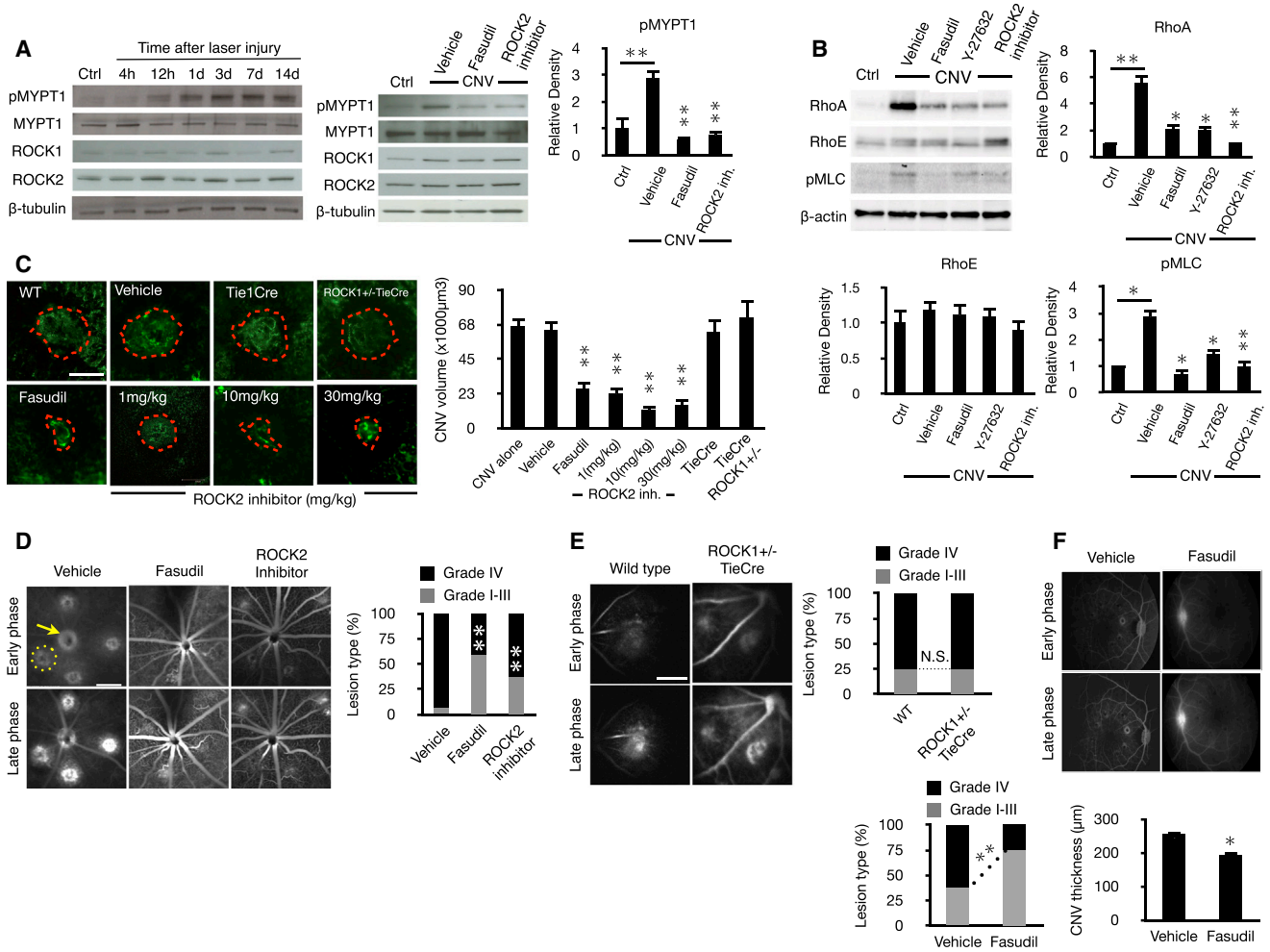

Figure 2. CNV Depends on ROCK Signaling

ROCK signaling was quantified in experimentally induced CNV and the effect of ROCK inhibition was studied in vivo.

(A and B) Western blot analysis (A) using whole-cell lysates from choroids of normal and CNV eyes at the indicated time points after laser injury. Vehicle and inhibitor-treated CNV eyes were screened at day 7 for anti-pMYPT1, anti-MYPT1, anti-ROCK1, anti-ROCK2, as well as (B) anti-RhoA, anti-RhoE, and anti-pMLC Abs, n = 3.

(C) Representative mouse CNV lesions treated with vehicle, fasudil (n = 5, 40 lesions), ROCK2 inhibitor at different concentrations (n = 4, 32 lesions in each group) and in ROCK1+/−TieCre mouse (n = 5, 40 lesions) with the corresponding quantifications. Red dashed line shows the extent of the laser-induced CNV lesions filled with FITC-dextran in flat-mounted choroids. Scale bar represents 100 μm.

(D and E) Leakage from the angiogenic vessels (D) was visualized by FA and quantified in early-phase (1–2 min) and late-phase (6–8 min) angiograms of Brown Norway rats treated with vehicle, fasudil, or ROCK2 inhibitor, as well as (E) in ROCK1+/−TieCre mice. Yellow dashed circle shows the extent of the CNV lesions filled with fluorescein; yellow arrow indicates the optic nerve. The scale bar represents 1 mm. The percentage of lesions is graded as I, II, III, defined as no to moderate leakage, and IV, clinically relevant leakage (n = 4, 32 lesions).

(F) Fluorescent angiography in monkey and CNV thickness measurements with vehicle or fasudil treatment (n = 4). *p < 0.05; **p < 0.01. Error bars are SEM.

for CD80, CD206, or significant staining for neither ROCK isoform.

The time course of protein expression showed elevated IL-4 and CD163 levels in CNV through day 7 or day 14, respectively. CCR7 was unchanged, while CD80 was moderately higher in the first 3 days. Further, CCR3 that was previously reported to be higher in CNV (Takeda et al., 2009) remained unchanged at the examined time points (Figure 5B).

To characterize the kinetics of macrophage accumulation, we performed flow cytometry in normal and lasered mouse eyes during CNV development. The number of CD11b(+)CD80(+) M1-like macrophages increased on day 1 after laser injury and remained high through day 7. In the CNV model, angiogenesis starts 3 days after laser injury and peaks on day 7 (Ishibashi et al., 1987). We found a peak of CD11b(−)CD206(+) cells on day 2 after laser injury, which preceded the reported start of angiogenesis. On days 3 through 7, the percentage of CD11b(+)CD206(+) cells increased with a peak on day 7, coinciding with the maximum angiogenic response in the laser-injury model (Figure 5C). These data show that even though both

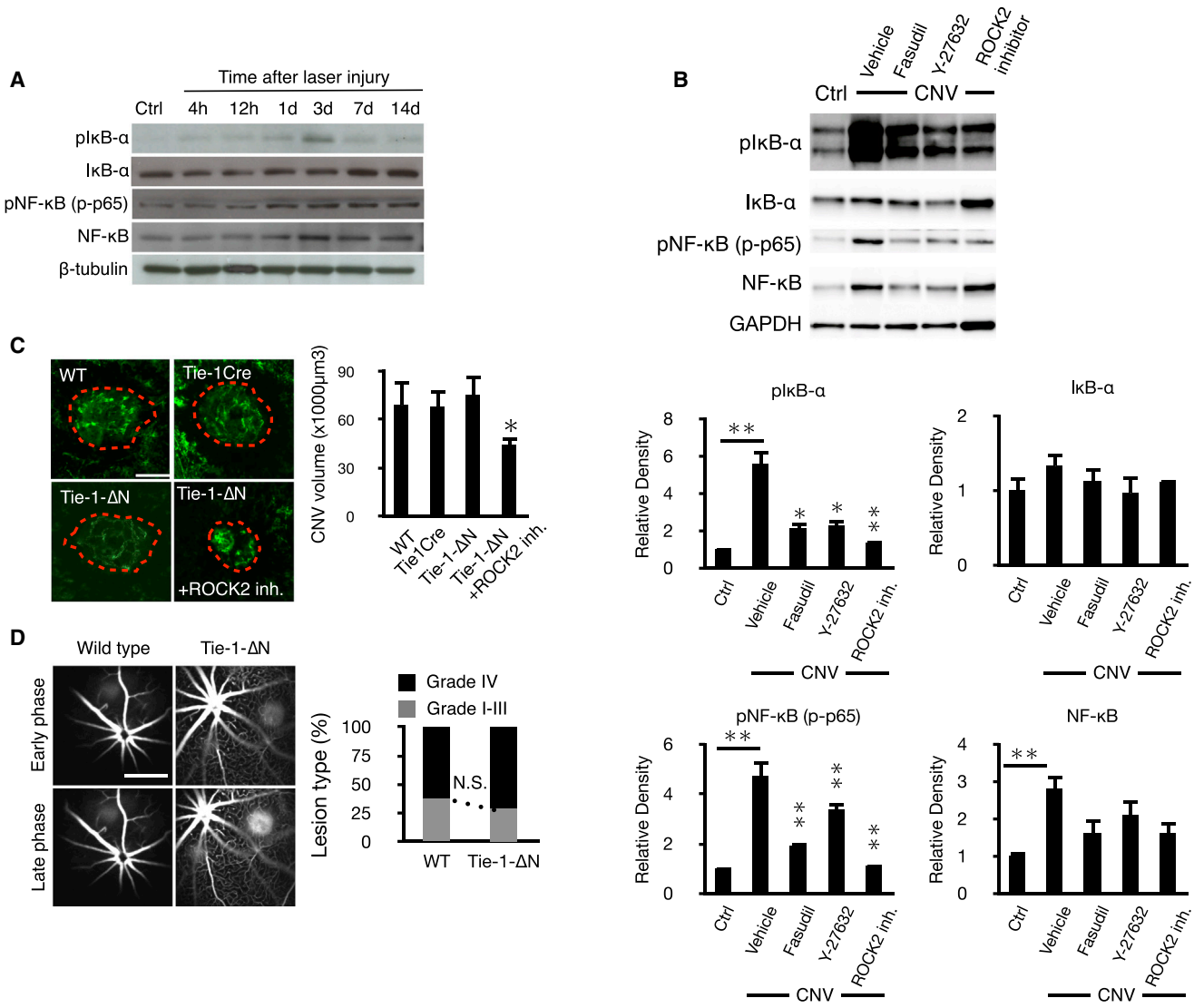

Figure 3. Lack of Endothelial NFκ-B Signaling Does Not Affect CNV

(A) Western blot analysis in whole-cell lysates of lasered eye extracts at different time points after laser injury.

(B) Representative western blot of anti-pIκB-α, anti-IκB-α, anti-pNF-κB p65, anti-NF-κB, anti-GAPDH with fasudil (20 mg/kg), Y-27632 (10 mg/kg), or ROCK2 inhibitor (10 mg/kg) treatment in choroids with CNV (day 7) with the corresponding quantifications.

(C) Representative micrographs of CNV lesions (day 7) in choroidal flat mounts from C57BL/6J, TieCre, or Tie-1-ΔN mice with or without ROCK2 inhibition. Scale bar represents 100 μm and quantitative analysis of CNV volume (n = 5 animals in each group, 40 lesions). *$p < 0.05$; **$p < 0.01$.

(D) Representative early phase (1–2 min) and late-phase (6–8 min) fluorescein angiograms in C57BL/6J and Tie-1-ΔN mice and quantification. Scale bar represents 1 mm. Error bars are SEM.

macrophage subtypes are found in CNV development, the accumulation kinetics of the M2-like macrophages closely matches the angiogenic response.

Dual ROCK1/2 and ROCK2 inhibition substantially decreased the CD11b(+)CD206(+) M2-like population when examined on day 7. The CD11b(+)CD206(−) cell population was reduced by dual ROCK1/2 inhibition but not by ROCK2 inhibition (Figure 5D).

ROCK Regulates Macrophage Polarization

To investigate the role of ROCK signaling in macrophage polarization, we stained for each isoform in macrophages (Figure 6A). In undifferentiated M0 macrophages ROCK1 and ROCK2 were evenly distributed in the cytoplasm. In M1 macrophages, ROCK1 was concentrated in the perinuclear regions. In comparison, ROCK2 was distributed in the cytoplasm. The cytoplasmic distribution of ROCK2 in M1 macrophages showed unique circular areas of nonexpression reminiscent of vacuoles. In M2 macrophages, ROCK1 was evenly distributed in the cytoplasm, while ROCK2 was highly concentrated near the nucleus.

To elucidate the role of ROCK in macrophage fate, we used genetic knockdown and pharmacological inhibition (Figure 6B).

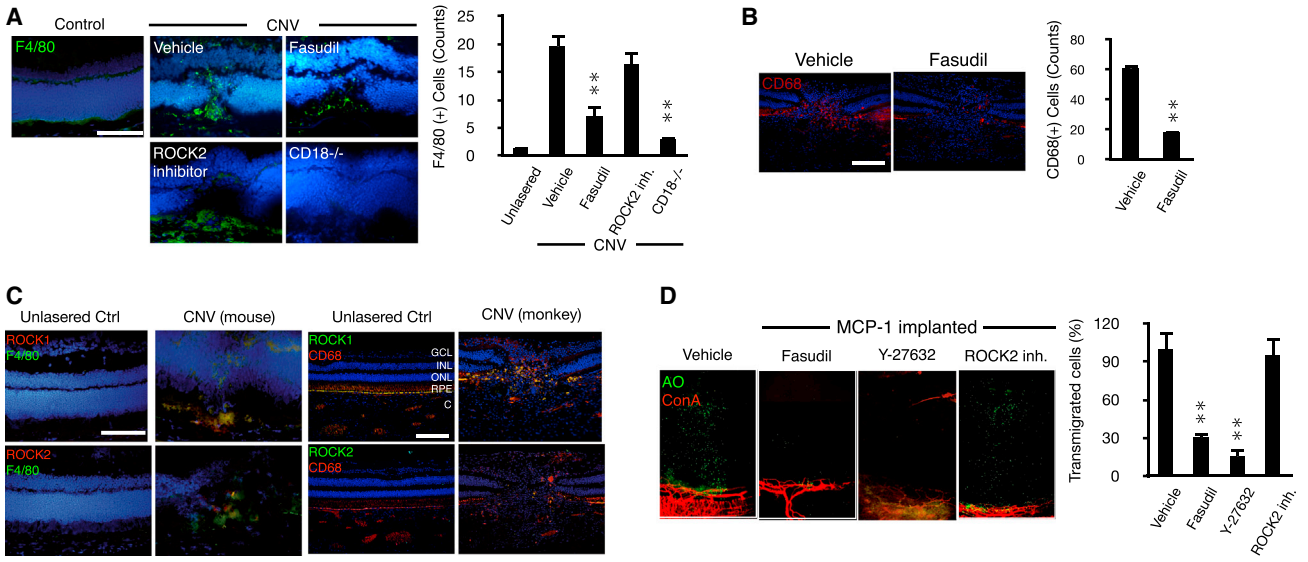

Figure 4. ROCK-Mediated Regulation of Inflammatory Leukocyte Infiltration during CNV

(A) Representative micrographs of laser-induced CNV lesions, immunostained for F4/80 in C57BL/6J mice treated with vehicle, fasudil, or ROCK2 inhibitor or in *CD18−/−* mice and quantification of the number of F4/80-positive macrophages in CNV lesions (n = 3 animals in each group). In each eye, six lesions were placed. From each lesion, ten or more sections were stained, the results of which were averaged for each lesion/animal. Scale bar represents 100 μm.

(B) Impact of fasudil on macrophage infiltration in laser-induced CNV in monkey (n = 4). This shows representative micrographs of CNV lesions, immunostained for CD68 in lasered monkeys treated with vehicle or fasudil and quantification of the number of CD68-positive leukocytes in CNV lesions (n = 4). **p < 0.01. Scale bar represents 100 μm.

(C) Double immunostaining of laser-induced CNV in monkey and mice with Abs of ROCK1 or ROCK2 and CD68 or F4/80. GCL, ganglion cell layer; INL, inner nuclear layer; ONL, outer nuclear layer; RPE, retinal pigmented epithelial layer; C, choroid. Scale bar represents 50 μm

(D) Ex vivo imaging of impact of ROCK inhibitors on MCP-1-mediated leukocyte transmigration. AO(+) leukocytes and Con A(+) angiogenic vessels in MCP-1-implanted corneas, 2 hr after AO injection, 24 hr after pellet implantation with vehicle, fasudil, Y-27632, or ROCK2 inhibitor treatment. This shows quantification of the number of AO(+) leukocytes in areas of MCP-1-implanted corneas 2 hr after AO injection, 24 hr after pellet implantation; n = 4; *p < 0.05, **p < 0.01. Error bars are SEM.

In M0 cells, ROCK2 knockdown increased CCL3, while ROCK1 knockdown increased CCL22. In an M1 environment, ROCK2 inhibition decreased IL-10 secretion, while it increased CCL5. In an M2 environment, ROCK1 knockdown increased CCL22 secretion. Both dual ROCK1/2 and selective ROCK2 inhibition reduced IL-10 secretion. Furthermore, dual ROCK1/2 and selective ROCK2 inhibition reduced the percentage of CD206(+) cells in flow cytometry, while ROCK2 inhibition increased the percentage of CD80(+) cells.

In bone marrow-derived M2 macrophages, dual ROCK1/2 and selective ROCK2 inhibition reduced Fizz 1 and Ym 1. In comparison, only ROCK2 inhibition but not dual ROCK1/2 inhibition reduced arginase 1. In contrast, ROCK2 inhibition significantly increased iNOS expression in RT-PCR. These data indicate a previously unknown regulatory role for ROCK isoforms in macrophage polarization (Figure 6C).

Pharmacologic inhibition of ROCK or knockdown of ROCK isoforms did not affect VEGF-A expression (Figure S5).

Causal Role of M2 Macrophages in Choroidal Neovascularization

To examine the contribution of macrophage subtypes in CNV formation, we differentiated murine bone marrow-derived macrophages into M1 or M2 phenotype (Figure S6) and injected them into the vitreous of laser-treated WT mice. While undifferentiated macrophages did not affect CNV, M2 macrophages increased the lesion size, not however in ROCK2 inhibitor-treated animals. In comparison, M1 macrophages reduced CNV lesions. Intravitreal injection of M1 macrophages in lasered mice that were treated with the ROCK2 inhibitor did not reduce lesion size any further, indicating that the beneficial effect of ROCK2 inhibition in vivo is indeed through macrophage polarization (Figure 7A).

Next, WT animals were intravitreally injected with M1 (INF-γ and LPS) or M2 (IL-4, IL-10, and IL-13) transforming cytokine cocktails. Intravitreal injection of INF-γ and LPS reduced CNV size and leakage. CNV and leakage in the M1-cytokine cocktail injected eyes remained unaffected when the animals were in addition ROCK2 inhibitor treated.

In contrast, intravitreal injection of IL-4, IL-10, and IL-13 increased CNV size and the percentage of clinically relevant IV leakage, which were reduced to control levels when the animals were in addition ROCK2 inhibitor treated (Figures 7B and 7C). These results indicate the importance of the cytokine profile in CNV, mediated through ROCK signaling.

M2-skewed IL-12p40−/− mice showed larger CNV lesions than WT animals. In contrast, M1-skewed adiponectin−/− mice had smaller CNV lesions than WT. These results show that an endogenous bias for macrophage subtypes affects CNV.

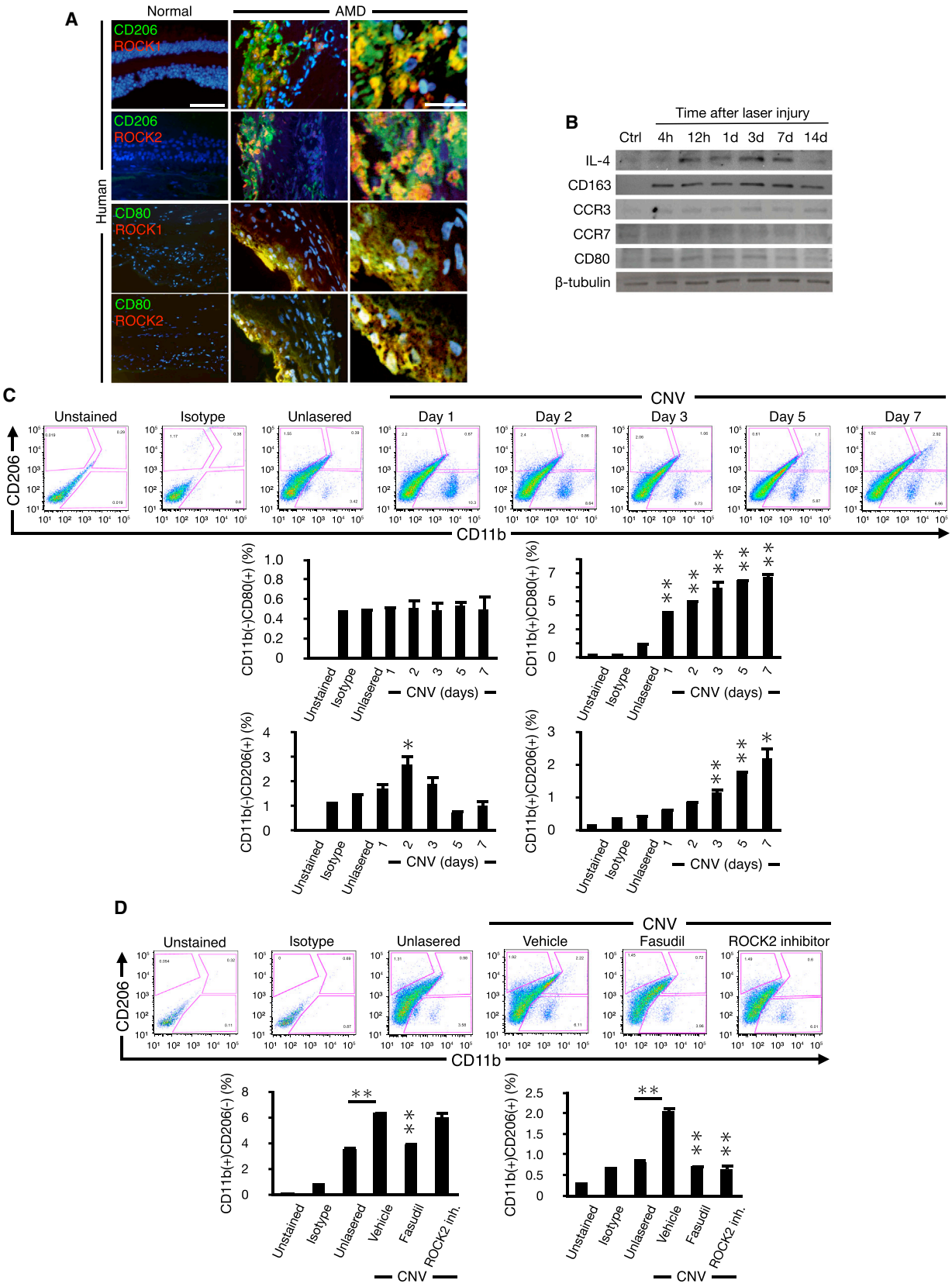

(legend on next page)

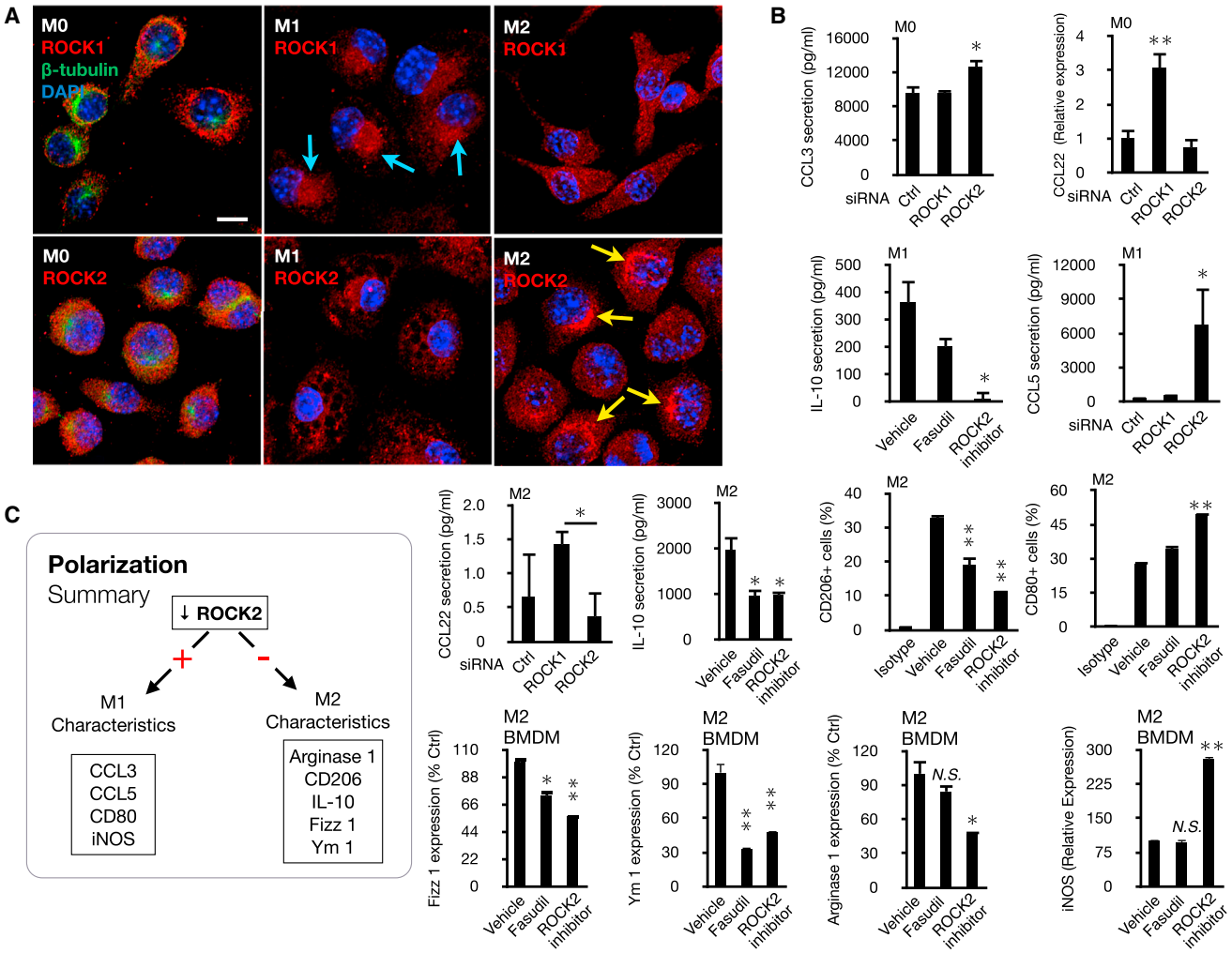

Figure 6. Isoform-Specific Inhibition of ROCK Determines Macrophage Fate

(A) Cellular localization of ROCK isoforms in polarized macrophages (M0, M1, M2). RAW 264.7 cells were differentiated into M0, M1, and M2 by cytokine treatment and used for immunostaining with Abs against ROCK1 or ROCK2 (red), β-tubulin (green) and DAPI (blue). Arrowheads, vacuoles. Scale bar represents 10 μm. In a small number of M1 cells, ROCK2 was also found more concentrated around the nucleus.

(B) ROCK isoforms were blocked in RAW 264.7, U937, and BMDM cells in M0, M1, or M2 environments. Chemokines, cell markers, and genes were quantified by luminex, flow cytometry, or RT-PCR. Data represent average from three or more independent experiments. RT-PCR data were evaluated after subtraction of the specific endogenous control gene expression (18S rRNA). *$p < 0.05$; **$p < 0.01$. Error bars indicate SEM.

(C) Schematic overview of how ROCK signaling impacts polarization.

While ROCK2 inhibition significantly reduced CNV size in IL-12p40−/− mice, it did not do the same in adiponectin−/− mice (Figure 7D). The efficacy of ROCK2 inhibition in IL-12p40−/− mice and the lack of it in adiponectin−/− mice further support the finding that the beneficial effects of ROCK2 inhibition are through a shift in macrophage polarization.

Figure 5. Polarization of Ocular Infiltrating Macrophages by ROCK

(A) Double immunostaining of normal human retina-choroidal complex and AMD membranes with Abs against CD206 or CD80 (green) and ROCK1 or ROCK2 (red) (n = 4). Overview bar represents 50 μm; high magnification, 20 μm.

(B) Western blot analysis with anti-IL-4, anti-CD163, anti-CCR3, anti-CCR7, anti-CD80 or anti-β-tubulin Abs, using whole-cell lysates from lasered mouse choroids at the indicated time points after injury. Other proteins from the same experiment shown in Figure 2A.

(C) FACS analysis of infiltrating cells from untreated and laser-injured choroids at the different time points after laser injury. Cells were stained for CD11b, CD80, and CD206. The percentages of infiltrating CD11b(+)CD206(+), CD11b(+)CD80(+), CD11b(−)CD206(+), CD11b(−)CD80(+) cells in CNV are shown at the indicated times (n = 6).

(D) FACS analysis of infiltrating cells from CNV eyes (choroid) with vehicle, fasudil, or ROCK2 inhibitor treatment at day 7 with PE-CD11b mAb and FITC-CD206 mAb. The percentages of infiltrating CD11b(+)CD206(+) cells and CD11b(+)CD206(−) cells in CNV are shown with the treatment at day 7 (n = 6). *$p < 0.05$; **$p < 0.01$. Error bars are SEM.

Age Compounded ROCK Signaling and an M2 Shift

To investigate ROCK signaling as a function of age, we quantified ROCK isoforms, their downstream mediators, and macrophage markers in the choroids of young (8- to 12-week-old) and aged (>16-month-old) WT mice with and without laser injury. Compared with the baseline in the normal young, MYPT1- and IκB-α phosphorylation were higher in the lasered young and in the normal-aged animals, with the highest levels found in the aged lasered animals, suggesting a compounding effect of age. In comparison, MYPT1 and IκB-α protein expressions did not differ between the groups (Figure 7E).

IL-4 was elevated in the young WT animals with CNV compared with the base levels in the normal young eyes. Unlasered aged WT mice had higher IL-4 levels compared with young WT animals even with CNV. Interestingly, the highest IL-4 level was found in the unlasered aged animals. CD163 was exclusively increased in CNV, while it was not affected by age in the normal eyes. The M1-specific markers CCR7 and CD80 were at similar levels in young and aged animals with or without laser injury (Figure 7E). However, in contrast to prior report (Takeda et al., 2009), CCR3 protein was unchanged in the eyes with CNV (Figure S7).

The higher levels of IL-4 in CNV were reversed by dual ROCK1/2 or selective ROCK2 inhibition. ROCK2 inhibition but not dual ROCK1/2 inhibition increased the M1 markers CD80 and CCR7 in lasered eyes (Figure 7F).

DISCUSSION

We introduce ROCK signaling as a master switch in macrophage polarization and suggest that M2-like macular-degeneration-associated macrophages (MaDAMs) are a cause of disease. Paradoxically, macrophages have been reported to promote CNV (Tsutsumi et al., 2003) and also to inhibit CNV (Apte et al., 2006), without elucidating which macrophage subtypes might be involved. Our work resolves this apparent discrepancy and illuminates how macrophages can both decrease and increase CNV, depending on their phenotype. When injected into the vitreal cavity, M1-like macrophages reduced while M2-like macrophages increased CNV. While both cell types were found in laser-injured mouse choroids, the accumulation kinetics of M2-like macrophages match the angiogenic response. Smaller CNV lesions in M1-skewed adiponectin−/− mice, in contrast to the larger lesions in the M2-skewed IL-12p40−/− mice, further bolstered the key role for macrophage polarization in CNV. ROCK2 inhibition suppressed M2 and furthered M1 polarization while ROCK1 inhibition furthered M2 polarization.

In mouse, monkey, and human, ROCK expression and signaling were associated with CNV. In human AMD membranes, angiogenic but not normal vessels expressed ROCK isoforms, making them candidate biomarker. Phosphorylation of downstream mediators of ROCK—MLC, MYPT1, IκB-α, and NF-κB p65—was increased in CNV and suppressed with dual ROCK1/2 or selective ROCK2 inhibition, indicating a key role for this pathway in CNV. NF-κB protein expression was higher in CNV, possibly due to immune cell accumulation. While we excluded a role for endothelial NF-κB in CNV, NF-κB activity in immune cells could be decisive in AMD. Dual ROCK1/2 and selective ROCK2 inhibition significantly reduced CNV, albeit through different mechanisms. We found ROCK1 signaling to be required for macrophage extravasation, while ROCK2 inhibition did not affect recruitment. Upstream of ROCK, RhoA was increased in CNV and reduced to normal levels with ROCK inhibition.

MaDAMs accumulate in AMD, possibly due to changes in the chorioretinal microenvironment with age. A potential cause could be IL-4, which we found increased with age. ROCK2 inhibition reduced IL-4 to baseline levels in CNV, thereby affecting the cytokine microenvironment in which macrophages differentiate in addition to directly shifting the macrophage balance from M2 to M1. Interestingly, IL-4 was reported to suppress laser-induced CNV through release of soluble Flt-1 from macrophages (Wu et al., Association for Research in Vision and Ophthalmology, 2011), pointing out the potential of macrophage polarization and plasticity as therapeutic targets.

Analogous to tumor-associated macrophages (TAMs) that correlate with poor prognosis in cancer, MaDAMs could predict onset or severity of AMD, for instance if quantified by molecular imaging (Sun et al., 2014) or in the peripheral blood. Specifically, CD163 was only found in CNV, which could become a biomarker for exudative AMD. MaDAMs expressed both ROCK isoforms, and ROCK2 inhibition reduced their number in CNV without affecting total macrophage numbers. Selective ROCK2 but not dual ROCK1/2 inhibition increased M1 markers, CD80 and CCR7. This preserves the beneficial macrophages that are essential for retinal health (London et al., 2011) and simultaneously restores the balance between proangiogenic MaDAMs and their angiostatic counterparts.

Age increased ROCK signaling and the M2-type immune response, evidenced by elevated pMYPT1, pIκB-α, CCR3, and IL-4 in the choroids of senescent mice. In contrast, age did not affect the M1-type response. This establishes a novel link between age and macrophage polarization that could explain the angiogenic switch in AMD. In contrast to prior work, in which IL-10-treated macrophages failed to reduce CNV (Kelly et al., 2007), our results showed that M2-differentiated macrophages significantly increase CNV. Importantly, the mechanism shown in this work is distinct from the prior concept of differential recruitment of macrophage subtypes in CNV (Zhao et al., 2013) since ROCK2 does not affect macrophage recruitment.

Demand is high for a ROCK2-specific inhibitor (Riento and Ridley, 2003). This study introduces an orally available selective ROCK2 inhibitor, which lacks toxicity in human. The antagonistic role of ROCK isoforms in macrophage polarization suggests that more efficacy and fewer side effects are possible with isoform-specific inhibition. A benefit of selective ROCK2 inhibition compared with dual ROCK1/2 inhibition is the M1 upregulation in lesions since selective ROCK2 inhibition does not interfere with macrophage recruitment. Instead, by targeting macrophage plasticity, selective ROCK2 inhibition restores the immunological balance that prevails in the normal young eye. Compared with anti-VEGF-A agents that only treat late symptoms (Rofagha et al., 2013), targeting macrophage polarization addresses roots of the disease.

AMD is considered an inflammatory disease (Hollyfield et al., 2008), yet our results highlight its immune-modulatory nature.

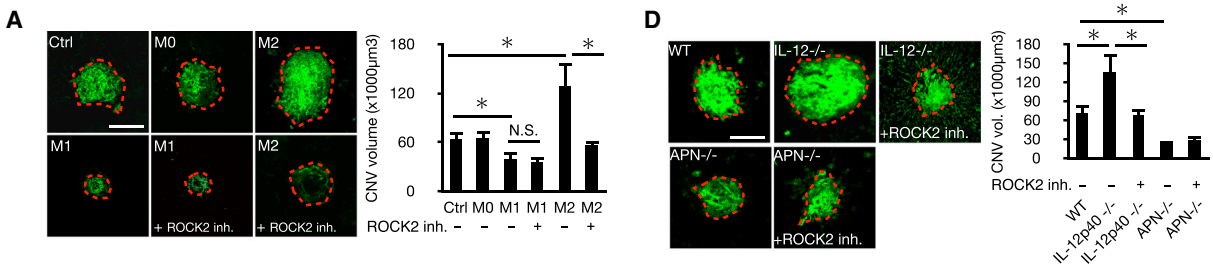

(legend on next page)

We found elevated NF-κB signaling in CNV that was suppressed with ROCK inhibition. NF-κB can be proangiogenic or antiangiogenic (Aurora et al., 2010). Since CNV was independent of endothelial NF-κB activity, yet pIκB-α was higher in aging and CNV, it is feasible that NF-κB's contribution to CNV is in immune cells. The causal role of macrophage polarization in CNV challenges the paradigm that AMD is inflammatory. Instead, rather than a sole phenotypic signature or a cell type, our results point toward immune imbalance as a root of AMD. These insights together with the considerable plasticity of macrophages open new prospects for immune-based therapy in age-related diseases. While macrophage polarization is a promising target, the complexity of the subject matter requires future insights to be fully understood.

This study introduces the role of ROCK in macrophage polarization. Aging increases ROCK2 signaling, resulting in overt expression of the proangiogenic MaDAMs. This newly revealed chain of events explains the angiogenic switch in the aging eye. In contrast, a shift of the fundus microenvironment toward M1, i.e., through selective ROCK2 inhibition, reduces the pathology and restores the physiological macrophage balance found in the young. These results facilitate the development of biomarkers for AMD and new immune-based therapies.

EXPERIMENTAL PROCEDURES

Human Tissues

Human CNV membranes were surgically excised from AMD and idiopathic neovascular maculopathy patients. The symptoms were documented as classic CNV, subfoveal or juxtafoveal CNV with hemorrhage and retinal detachment, when present. The average age for AMD patients (n = 7) was 71.3 years and for idiopathic neovascular maculopathy (n = 7) was 33.2 years. The average duration from the time of onset to surgery was 8.9 months. The average size of the CNV lesions was 0.84 of the disc diameter. Control eyes were from donor eyes without AMD. An institutional review board granted approval for allocation and histological analysis of specimens.

Animals

All animal experiments adhered to The Guiding Principles in the Care and Use of Animals (DHEW Publication, NIH 80-23).

Monkeys

Eyes from cynomolgus monkeys between 3 and 4 years of age were used in this study. General anesthesia was achieved by intramuscular injection of ketamine hydrochloride (20 mg/kg; Sankyo Yell Pharmaceutical Products).

Rodents

Male C57BL/6J mice (Stock# 000664; Jackson Laboratory) weighing 24–28 g were used. Jackson Laboratory tested and confirmed that their C57BL/6J production line is free of the *rd8* mutation. In addition, we tested the rd8 status of our experimental mice by PCR, the results of which showed that our experimental strains were free of the rd8 mutation in the Crb1 gene (Mattapallil et al., 2012) (Figure S8). The genetically modified mice used in this work were phenotypically normal and on C57BL/6J background. They did not differ in weight or age from their WT counter parts. Animals were sheltered in ventilated plastic cages in a temperature-controlled animal facility with a 12-hr light/dark cycle and were fed standard laboratory chow and water ad libitum. In this study, young WT were 8–12 weeks old, while aged animals were >16 months old. Male, 8- to 12-week-old adiponectin−/− and IL-12p40−/− mice were purchased from Jackson Laboratory. Adiponectin regulates M2 polarization and adiponectin−/− mice express more M1 cells (Ohashi et al., 2010). Macrophages from IL-12p40−/− mice have a bias toward the M2 phenotype (Bastos et al., 2002).

Tie1Cre/IκB-αΔN (Tie1ΔN) Mice. For this project, the IκB-αΔN (loxP-ΔN) mice were crossed with the Tie1Cre mice to generate the Tie1Cre/IκB-αΔN mice (or short Tie1ΔN) that were used for CNV experiments. As a result of the IκB-αΔN expression in the endothelial cells, these mice lack NF-κB signaling in their vascular endothelium. Noteworthy, Tie-1-Cre mice do not express Cre only in the vascular endothelial cells. There was a 12%–20% Cre expression in adult erythroid, myeloid, and lymphoid cells (Gustafsson et al., 2001).

The IκB-αΔN mice are knock-in mice. In brief, the cDNA of the human NF-κB suppressor IκB-αΔN was integrated by homologous recombination in frame into the β-catenin locus (Schmidt-Ullrich et al., 2001). In the floxed IκB-αΔN mice that were used in the current work, a loxP-stop-loxP cassette was cloned in front of the transgene, resulting in the human IκB-αΔN suppressor only to be expressed in the presence of Cre (Freund et al., 2005; Henke et al., 2007; Schmidt-Ullrich et al., 2001). IκB-αΔN was expressed in all tissues, consistent with the ubiquitous distribution of β-catenin.

The ROCK1+/−Tie1Cre Mice. To have ROCK1-deficient mice on a pigmented background, we generated tissue-specific haploinsufficient ROCK1-deficient mice on C57Bl/6J background. For this, Tie1-Cre ROCK1 LoxP/− (or endothelial-specific ROCK1-deficient mice) were generated by mating Tie1-Cre recombinase knock-in mice with ROCK1 LoxP/− mice (Huang et al., 2012). Heterozygote ROCK1+/− mice on C57Bl/6J background are viable and fertile with no obvious phenotypic abnormalities. They express ROCK1 in approximately half the amount of normal WT, while there is no compensatory upregulation of ROCK2 (Rikitake et al., 2005).

Cell Culture and Transfection

The monocyte cell line U937 (CRL-1593.2; ATCC) was maintained in RPMI-1640 supplemented with 10% fetal bovine serum (FBS) (Atlanta Biologicals), glutamine (2 mmol/L), penicillin (100 U/ml), and streptomycin (100 μg/ml; GIBCO, BRL). The mouse monocyte cell line RAW 264.7 (TIB-71; ATCC) was maintained in DMEM (30-2002; ATCC).

Transfections were performed using control (sc-37007), ROCK1 (sc-29473h, sc-36432 m), and ROCK2 (sc-29474h, sc-36433 m) siRNA from Santa Cruz Biotechnology via electroporation (VCA-1004 Amaxa).

Differentiation of Bone-Marrow-Derived Macrophages

Bone marrow cells were collected from femurs and tibias of WT C57Bl/6J mice. The cells were cultured in RPMI1640 medium supplemented with 20% FCS,

Figure 7. Age-Induced ROCK Signaling and M2 Differentiation Cause CNV

(A) Representative laser-induced CNV results from mice after intravitreal injections of vehicle, M0, M1, or M2 macrophages with or without ROCK2 inhibitor and the corresponding quantifications (n = 5 mice, 10 eyes). Scale bar represents 100 μm.

(B) Representative micrographs of CNV lesions from mice after intravitreal cytokine injections, M1 cocktail: INF-γ and LPS, M2 cocktail: IL-4, Il-10, IL13 and the corresponding quantifications. Scale bar represents 100 μm.

(C) Leakage from the angiogenic vessels was visualized by FA and quantified in early-phase (1–2 min) and late-phase (6–8 min) angiograms of mice injected with either M1 or M2 cocktail. Scale bar represents 1 mm.

(D) Representative micrographs of CNV lesions from C57BL/6J mice, IL-12p40−/− and adiponectin−/− mice with and without ROCK2 inhibitor and the corresponding quantifications. Scale bar represents 100 μm.

(E) Representative western blots of normal and CNV (day 3) choroids from young (8–12 weeks old) and aged (>16 months old) WT mice with the corresponding quantifications; n = 3, *$p < 0.05$; **$p < 0.01$.

(F) Representative western blots of anti-IL-4, anti-CD80, and anti-CCR7 with fasudil (20 mg/kg), Y-27632 (10 mg/kg), or ROCK2 inhibitor (10 mg/kg) treatments in choroids with CNV (day 7) with the corresponding quantifications. Error bars are SEM.

30% L cell sup (containing M-CSF) and P/S for 5 days. Bone marrow-derived macrophages (BMDMs) were stimulated with 1 μg/ml LPS and 20 ng/ml IFN-γ (M1 phenotype) or 20 ng/ml IL-4, IL-10, and IL-13 (M2 phenotype) for 24 hr. BMDMs were collected and washed with PBS/2 mM EDTA (cold), incubated with 5μg/ml anti-FcγR mAb (2.4G2), followed by staining with 2.5 μg/ml CD80-FITC, CD206-FITC, or isotype control. After washing with PBS/EDTA, BMDMs were analyzed using a flow cytometer (FACS Calibur).

Immunohistochemistry

Paraffin-embedded sections of human eyes were deparaffinized and rehydrated with a graded alcohol series. Immunofluorescent staining was performed with antibodies (Abs) against human vWF (F3520; Sigma), human macrophage mannose receptor (MMR) (CD206, MAB2534, R&D Systems), human CD80 (ab53003; Abcam), or human ROCK1 (sc-17794; Santa Cruz Biotechnology) or ROCK2 (sc-1851; Santa Cruz Biotechnology) and identified with Alexa Fluor 488 (10μg/ml, A-11055; Invitrogen) or 647 (10μg/ml, A21244; Invitrogen) secondary Abs. On day 3 after laser injury, 10 μm frozen sections of the posterior segment were prepared. The mouse eye sections were incubated with a rat antimouse F4/80 mAb (MCA497R, AbD Serotec) or CD11b (550282, BD PharMingen) and subsequently with the secondary Ab. In monkey eyes, CD68 (goat pAb, sc-7082; Santa Cruz), vWF (rabbit pAb, A0082; DAKO), ROCK1 (mouse mAb, sc-17794; Santa Cruz), and ROCK2 (goat pAb, sc-1851; Santa Cruz) were stained. Images were obtained with a Leica microscope.

Western Blot

To obtain tissues, animals were perfused with PBS, and eyes were enucleated immediately after perfusion. Choroid-retinal pigment epithelium (RPE) complex were microsurgically isolated and placed in 100 μl of lysis buffer (mammalian cell lysis kit MCL1; Sigma), supplemented with protease and phosphatase inhibitors (P2850, P5726, P8340; Sigma), and sonicated. The lysate was centrifuged (12,000 rpm, 15 min, 4°C), and the supernatant was collected. Each sample containing an equal amount of total protein, quantified by protein assay (Bio-Rad Laboratories), was separated by SDS-PAGE and electroblotted to polyvinylidene difluoride (PVDF) membranes (Invitrogen). To block nonspecific binding, the membranes were washed with 5% skim milk and subsequently incubated with the following: rabbit Abs against phospho-MBS/MYPT1-THr853 (CY-P1025; Cyclex), MYPT1 (sc-25618; Santa Cruz Biotechnology), phospho NF-κB p65 (3033; Cell Signaling), NF-κB p65 (3034; Cell Signaling), IκB-α (9242; Cell Signaling) or mouse Abs against pIκB-α (9246; Cell Signaling), ROCK1 and ROCK2 (611136, 610623; BD Transduction Laboratories), phosphorylated ezrin/radixin/moesin (pERM) (3149; Cell Signaling), ERM (3142; Cell Signaling), phosphorylated myosin light chain (pMLC) (3675, Cell Signaling), MLC (8505; Cell Signaling), IL-4 (ab11524; Abcam), CD163 (sc-33560; Santa Cruz Biotechnology), CCR3 (ab32512; Abcam), CCR7 (ab65851; Abcam), CD80 (ab53003; Abcam), and β-tubulin (ab11308; Abcam) at 4°C overnight, followed by incubation with a horseradish peroxidase-conjugated donkey or sheep Ab against rabbit or mouse IgG (NA934V, NXA931; GE Healthcare) or goat anti-rat secondary Ab (goat anti-rat IgG-HRP: sc-2032; Santa Cruz). The signals were visualized by chemiluminescence (ECL kit; GE Healthcare).

Real-Time RT-PCR

Total RNA from cultured RAW 264.7 cells was extracted using the RNeasy Plus Mini Kit (74134; Quiagen); 600 ng cDNA per sample was synthesized with TaqMan Reverse Transcription Reagents (N808-0234; Applied Biosystems) using its contained random hexamers scaled for a reaction volume of 30 μl. Quantitative real-time PCR was performed with the TaqMan Universal PCR Master Mix (4324018; Applied Biosystems) and the respective probes: CCL22 (Hs00171080_m1; Applied Biosystems), VEGF-A (Mm01281449_m1; TaqMan), and 18S rRNA (Hs99999901_s1; Applied Biosystems) as endogenous control.

In BMDM experiments, cDNA was synthesized from total RNA with Quantiscript Reverse Transcriptase and optimized blend of oligo-dT and random primers (Millipore). Gene expression was measured by the change-in-threshold ($\Delta\Delta C_T$) method based on quantitative real-time PCR in a Light Cycler (Roche) with SYBR Green I.

The primer sets for the murine Arg1 (Arginase-1; forward, cctgaaggaactgaaaggaaag, reverse, ttggcagatatgcagggagt), Retnla (Fizz1; forward, ccctc cactgtaacgaagactc, reverse, cacacccagtagcagtcatcc), Chi3l3 (Ym1; forward, gaacactgagctaaaaactctcctg, reverse, gagaccatggcactgaacg) and Nos2 (iNOS; forward, gggctgtcacggagatca, reverse, ccatgatggtcacattctgc), β-Actin (Actb; forward, catccgtaaagacctctatgccaac, reverse, accagaggcatacagg gaca) were used. Experiments were performed using Applied Biosystem's Step One Plus real-time PCR system using the company's standard cycles. The relative abundance of transcripts was normalized according to that of mouse GAPDH (4352932; Applied Biosystems), 18S rRNA.

Flow Cytometry

To examine macrophages in the retina and choroid, cells were prepared from mouse eyes. To collect a sufficient number of ocular infiltrating cells, 50 burns were delivered to mouse eyes by laser. After laser injury, eyes were enucleated at different time points (1, 2, 3, 5, and 7 days). The anterior segment (cornea, iris, and lens) was excised, and the posterior segment of the eye, including sclera, choroid, and retina, was disrupted with scissors and then shaken in DMEM (plus 10% FBS; GIBCO Laboratories; 100 U/ml penicillin, 100 μg/ml streptomycin) supplemented with 0.5 mg/ml collagenase type D (11088874103; Boehringer Mannheim) at 37°C for 60 min. The supernatants were collected and passed through a mesh. After three washes, viable cells were obtained. A total of 12 eyes (six individual pools) was examined per group. The cells were stained with PE anti-mouse CD11b (557397; BD PharMingen), FITC anti-mouse CD206 (MMR, 123005; BioLegend), and PE-Cy5 anti-mouse CD80 Abs (15-0801-81; eBioscience).

RAW 264.7 cells were stained with PerCP anti-mouse CD11b (101230; BioLegend), PerCP anti-mouse F4/80 (123006; BioLegend), PE anti-mouse CD80 (12-0801; eBioscience), and FITC anti-mouse CD206 (141704; BioLegend).

Laser-Induced CNV

Laser-induced CNV is a wound-healing model that mimics the angiogenesis and leakage aspects of AMD (Ishibashi et al., 1987). To induce CNV, C57BL/6J mice were anesthetized, and pupils were dilated with 5% phenylephrine and 0.8% tropicamide. Using a 532-nm laser (Oculight GLx, Iridex), a slit-lamp delivery system, and a cover glass as a contact lens, four spots (100 mW, 50 μm, 100 ms) were placed in each eye. The lesions were located at 3, 6, 9, and 12 o'clock meridians centered on the optic nerve head and two to three disk diameters from the optic nerve head. The same technique was used in cynomolgus monkeys (700 mW, 100 μm, 100 ms). Development of a bubble under laser radiation confirmed the rupture of the Bruch's membrane. Eyes showing hemorrhage were excluded from experiments.

Quantification of CNV and Leakage

At 7 or 14 days after laser injury, the size of CNV lesions was measured in choroidal flat mounts. Briefly, mice were anesthetized and perfused through the left ventricle with PBS, followed by 5 ml of 5% fluorescein isothiocyanate-dextran (FD2000S; Sigma Aldrich) in 1% gelatin. The anterior segment and retina were removed from the eyecup. The remaining RPE-choroid-sclera complex was flat mounted, after relaxing radial incisions, using Mounting Medium (FM 100119, Thermo Scientific) and coverslips. Micrographs of the choroidal complex were taken with a Leica Microscope. The volume of the lesions was quantified, using confocal microscopy (Leica TCS SP2 laser scanning confocal microscope). The magnitude of the CNV lesions was determined by measuring the hyperfluorescent area with Openlab Software (Improvision). The grade of leakage was determined by fluorescein angiography (FA).

FA

FA was performed in anesthetized rodents, mice (C57BL/6J) and rats (Brown Norway), using a digital fundus camera (SLO; HRA2; Heidelberg Engineering) 7 and 14 days after laser injury. Fluorescein injections were performed intravenously (0.2 ml of 2% fluorescein; Akorn, NDC 17478-253-10). For FA in monkeys, animals were injected with 5% fluorescein intravenously (Fluorescite, Alcon). FA images were evaluated by two masked retina specialists. The grading criteria were grade I, no hyperfluorescence; grade II, hyperfluorescence without leakage; grade III, hyperfluorescence in the early or midtransit images and late leakage; grade IV, bright hyperfluorescence in the transit images and late leakage beyond the treated areas. The grade IV lesions were considered clinically significant (Lara-Castillo et al., 2009).

Treatments

To block both ROCK isoforms, the dual ROCK1/2 inhibitors, fasudil (20mg/kg, H-2330; LC Laboratories; molecular weight [MW], 364.29) and Y-27632 (10 mg/kg, S1049, http://www.selleckchem.com) were administered daily by intraperitoneal injections. To block ROCK2, mice received twice daily intraperitoneal injections of the selective ROCK2 inhibitor (10 mg/kg, SurfaceLogix, MW, 570.61). The ROCK2 selective inhibitor, is currently being developed for clinical use by Kadmon (Kadmon) under the designation KD025. The control animals received equivalent amounts of vehicle, glyceryl trioctanoate (91039; Sigma-Aldrich). Intravitreal injections of fasudil and ROCK2 inhibitor (5 μl in rat and 1 μl in mouse; 30 μmol/l) were performed on days 0, 3, and 6 after CNV induction, using BSS Plus as vehicle. Adult cynomolgus monkeys received intravitreous injection of fasudil (30 μmol/l) three times per week.

The inhibitor treatments, unless indicated otherwise, started on day 0 at the same time as CNV induction and continued daily (fasudil once per day, ROCK2 inhibitor twice per day) until harvest.

Statistical Analysis

All values are expressed as mean ± SEM. Data were analyzed by Student's t test, ANOVA, or chi-square test. Differences between the experimental groups were considered statistically significant (*) or highly significant (**), when the p was < 0.05 or < 0.01, respectively.

SUPPLEMENTAL INFORMATION

Supplemental Information includes seven figures and can be found with this article online at http://dx.doi.org/10.1016/j.celrep.2015.01.050.

AUTHOR CONTRIBUTION

S.Z. and S.N. performed the majority of the experiments and analyzed the results. A.H.-M. designed the study, coordinated collaborations, supervised the experimental work, and wrote the manuscript. All authors read and approved of the manuscript.

ACKNOWLEDGMENTS

We thank Sonja Frimmel, Sepideh Faez, Lola Chabtini, and Roberto Bassi for technical assistance and Rebecca Garland for critical review of the manuscript. Randy Huang and David M. Dombkowski (Center for Regenerative Medicine and Technology, Massachusetts General Hospital) assisted with flow cytometry. We thank Professor K.C. Hayes for his commitment to mentorship. This work was supported by NIH/National Institute of Diabetes and Digestive and Kidney Diseases through Diabetes Complications Consortium award 25732-30 (A.H.-M.), the BrightFocus Foundation, the Malaysian Palm Oil Board (A.H.-M.), and R01DK083567 (Y.-B.K.). Grants are from JSPS KAKENHI, Grant-in-Aid for Young Scientists (A) (#25713057 to S.N.). E.K., O.S., S.C., and P.S. were employed by SurfaceLogix, a company that developed the selective small molecule inhibitor against ROCK2, which was used in this work.

Received: June 16, 2014
Revised: October 6, 2014
Accepted: January 20, 2015
Published: February 19, 2015

REFERENCES

Apte, R.S., Richter, J., Herndon, J., and Ferguson, T.A. (2006). Macrophages inhibit neovascularization in a murine model of age-related macular degeneration. PLoS Med. *3*, e310.

Arita, R., Hata, Y., Nakao, S., Kita, T., Miura, M., Kawahara, S., Zandi, S., Almulki, L., Tayyari, F., Shimokawa, H., et al. (2009). Rho kinase inhibition by fasudil ameliorates diabetes-induced microvascular damage. Diabetes *58*, 215–226.

Aurora, A.B., Biyashev, D., Mirochnik, Y., Zaichuk, T.A., Sánchez-Martinez, C., Renault, M.A., Losordo, D., and Volpert, O.V. (2010). NF-kappaB balances vascular regression and angiogenesis via chromatin remodeling and NFAT displacement. Blood *116*, 475–484.

Bastos, K.R., Alvarez, J.M., Marinho, C.R., Rizzo, L.V., and Lima, M.R. (2002). Macrophages from IL-12p40-deficient mice have a bias toward the M2 activation profile. J. Leukoc. Biol. *71*, 271–278.

Cammarano, M.S., and Minden, A. (2001). Dbl and the Rho GTPases activate NF kappa B by I kappa B kinase (IKK)-dependent and IKK-independent pathways. J. Biol. Chem. *276*, 25876–25882.

Cao, X., Shen, D., Patel, M.M., Tuo, J., Johnson, T.M., Olsen, T.W., and Chan, C.C. (2011). Macrophage polarization in the maculae of age-related macular degeneration: a pilot study. Pathol. Int. *61*, 528–535.

Chun, K.H., Araki, K., Jee, Y., Lee, D.H., Oh, B.C., Huang, H., Park, K.S., Lee, S.W., Zabolotny, J.M., and Kim, Y.B. (2012). Regulation of glucose transport by ROCK1 differs from that of ROCK2 and is controlled by actin polymerization. Endocrinology *153*, 1649–1662.

Freund, C., Schmidt-Ullrich, R., Baurand, A., Dunger, S., Schneider, W., Loser, P., El-Jamali, A., Dietz, R., Scheidereit, C., and Bergmann, M.W. (2005). Requirement of nuclear factor-kappaB in angiotensin II- and isoproterenol-induced cardiac hypertrophy in vivo. Circulation *111*, 2319–2325.

Gustafsson, E., Brakebusch, C., Hietanen, K., and Fässler, R. (2001). Tie-1-directed expression of Cre recombinase in endothelial cells of embryoid bodies and transgenic mice. J. Cell Sci. *114*, 671–676.

Henke, N., Schmidt-Ullrich, R., Dechend, R., Park, J.K., Qadri, F., Wellner, M., Obst, M., Gross, V., Dietz, R., Luft, F.C., et al. (2007). Vascular endothelial cell-specific NF-kappaB suppression attenuates hypertension-induced renal damage. Circ. Res. *101*, 268–276.

Hollyfield, J.G., Bonilha, V.L., Rayborn, M.E., Yang, X., Shadrach, K.G., Lu, L., Ufret, R.L., Salomon, R.G., and Perez, V.L. (2008). Oxidative damage-induced inflammation initiates age-related macular degeneration. Nat. Med. *14*, 194–198.

Huang, H., Kong, D., Byun, K.H., Ye, C., Koda, S., Lee, D.H., Oh, B.C., Lee, S.W., Lee, B., Zabolotny, J.M., et al. (2012). Rho-kinase regulates energy balance by targeting hypothalamic leptin receptor signaling. Nat. Neurosci. *15*, 1391–1398.

Ishibashi, T., Miller, H., Orr, G., Sorgente, N., and Ryan, S.J. (1987). Morphologic observations on experimental subretinal neovascularization in the monkey. Invest. Ophthalmol. Vis. Sci. *28*, 1116–1130.

Kelly, J., Ali Khan, A., Yin, J., Ferguson, T.A., and Apte, R.S. (2007). Senescence regulates macrophage activation and angiogenic fate at sites of tissue injury in mice. J. Clin. Invest. *117*, 3421–3426.

Klein, R., Klein, B.E., Tomany, S.C., Meuer, S.M., and Huang, G.H. (2002). Ten-year incidence and progression of age-related maculopathy: The Beaver Dam eye study. Ophthalmology *109*, 1767–1779.

Lara-Castillo, N., Zandi, S., Nakao, S., Ito, Y., Noda, K., She, H., Ahmed, M., Frimmel, S., Ablonczy, Z., and Hafezi-Moghadam, A. (2009). Atrial natriuretic peptide reduces vascular leakage and choroidal neovascularization. Am. J. Pathol. *175*, 2343–2350.

London, A., Itskovich, E., Benhar, I., Kalchenko, V., Mack, M., Jung, S., and Schwartz, M. (2011). Neuroprotection and progenitor cell renewal in the injured adult murine retina requires healing monocyte-derived macrophages. J. Exp. Med. *208*, 23–39.

Mantovani, A., Sica, A., Sozzani, S., Allavena, P., Vecchi, A., and Locati, M. (2004). The chemokine system in diverse forms of macrophage activation and polarization. Trends Immunol. *25*, 677–686.

Mattapallil, M.J., Wawrousek, E.F., Chan, C.C., Zhao, H., Roychoudhury, J., Ferguson, T.A., and Caspi, R.R. (2012). The Rd8 mutation of the Crb1 gene is present in vendor lines of C57BL/6N mice and embryonic stem cells, and confounds ocular induced mutant phenotypes. Invest. Ophthalmol. Vis. Sci. *53*, 2921–2927.

Ohashi, K., Parker, J.L., Ouchi, N., Higuchi, A., Vita, J.A., Gokce, N., Pedersen, A.A., Kalthoff, C., Tullin, S., Sams, A., et al. (2010). Adiponectin promotes

macrophage polarization toward an anti-inflammatory phenotype. J. Biol. Chem. *285*, 6153–6160.

Riento, K., and Ridley, A.J. (2003). Rocks: multifunctional kinases in cell behaviour. Nat. Rev. Mol. Cell Biol. *4*, 446–456.

Rikitake, Y., Oyama, N., Wang, C.Y., Noma, K., Satoh, M., Kim, H.H., and Liao, J.K. (2005). Decreased perivascular fibrosis but not cardiac hypertrophy in ROCK1+/- haploinsufficient mice. Circulation *112*, 2959–2965.

Rofagha, S., Bhisitkul, R.B., Boyer, D.S., Sadda, S.R., and Zhang, K.; SEVEN-UP Study Group (2013). Seven-year outcomes in ranibizumab-treated patients in ANCHOR, MARINA, and HORIZON: a multicenter cohort study (SEVEN-UP). Ophthalmology *120*, 2292–2299.

Schmidt-Ullrich, R., Aebischer, T., Hülsken, J., Birchmeier, W., Klemm, U., and Scheidereit, C. (2001). Requirement of NF-kappaB/Rel for the development of hair follicles and other epidermal appendices. Development *128*, 3843–3853.

Sica, A., and Mantovani, A. (2012). Macrophage plasticity and polarization: in vivo veritas. J. Clin. Invest. *122*, 787–795.

Sun, D., Nakao, S., Xie, F., Zandi, S., Bagheri, A., Rezaei Kanavi, M., Samiei, S., Soheili, Z.S., Frimmel, S., Zhang, Z., et al. (2014). Molecular imaging reveals elevated VEGFR-2 expression in retinal capillaries in diabetes: a novel biomarker for early diagnosis. FASEB J., Published online June 5, 2014.

Tabruyn, S.P., and Griffioen, A.W. (2008). NF-kappa B: a new player in angiostatic therapy. Angiogenesis *11*, 101–106.

Takeda, A., Baffi, J.Z., Kleinman, M.E., Cho, W.G., Nozaki, M., Yamada, K., Kaneko, H., Albuquerque, R.J., Dridi, S., Saito, K., et al. (2009). CCR3 is a target for age-related macular degeneration diagnosis and therapy. Nature *460*, 225–230.

Tsutsumi, C., Sonoda, K.H., Egashira, K., Qiao, H., Hisatomi, T., Nakao, S., Ishibashi, M., Charo, I.F., Sakamoto, T., Murata, T., and Ishibashi, T. (2003). The critical role of ocular-infiltrating macrophages in the development of choroidal neovascularization. J. Leukoc. Biol. *74*, 25–32.

Zhao, H., Roychoudhury, J., Doggett, T.A., Apte, R.S., and Ferguson, T.A. (2013). Age-dependent changes in FasL (CD95L) modulate macrophage function in a model of age-related macular degeneration. Invest. Ophthalmol. Vis. Sci. *54*, 5321–5331.

Cell Reports

Supplemental Information

ROCK-Isoform-Specific Polarization of Macrophages Associated with Age-Related Macular Degeneration

Souska Zandi, Shintaro Nakao, Kwang-Hoon Chun, Paolo Fiorina, Dawei Sun, Ryoichi Arita, Ming Zhao, Enoch Kim, Olivier Schueller, Stewart Campbell, Mahdi Taher, Mark Ivan Melhorn, Alexander Schering, Francesca Gatti, Sara Tezza, Fang Xie, Andrea Vergani, Shigeo Yoshida, Keijiro Ishikawa, Muneo Yamaguchi, Fumiyuki Sasaki, Ruth Schmidt-Ullrich, Yasuaki Hata, Hiroshi Enaida, Mitsuko Yuzawa, Takehiko Yokomizo, Young-Bum Kim, Paul Sweetnam, Tatsuro Ishibashi, and Ali Hafezi-Moghadam

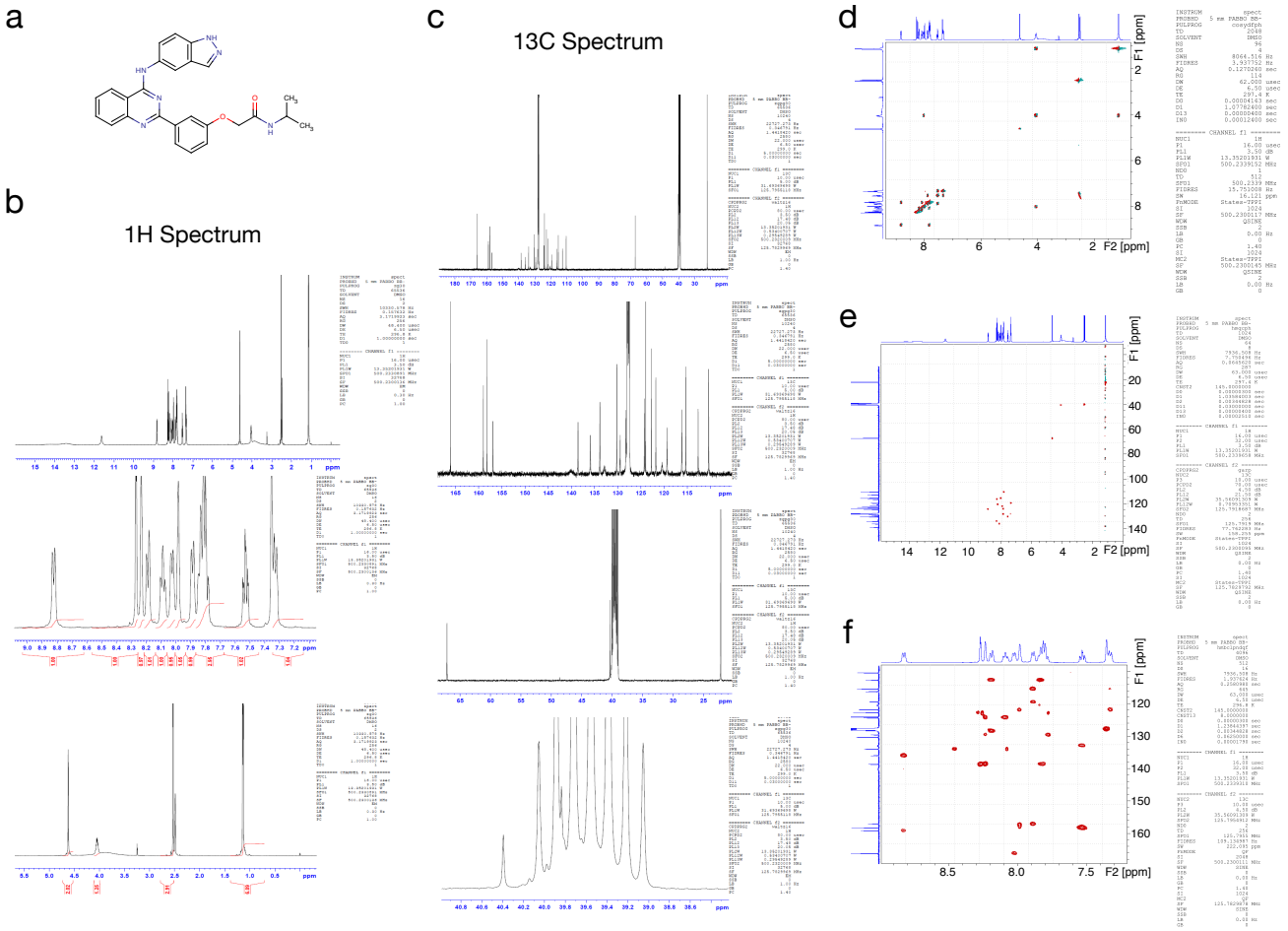

Supplemental Figure 1, related to Figure 2: Structure and nuclear magnetic resonance spectra of the ROCK2 inhibitor. (a) The selective ROCK2 inhibitor, 2-(3-(4-(1H-indazol-5-ylamino)quinazolin-2-yl)phenoxy)-N-isopropylacetamide (Sweetnam et al., 2010). **(b)** 1D 1H nuclear magnetic resonance (NMR) spectrum, **(c)** 1D 13C spectrum. **(d)** double-quantum-filtered correlation spectroscopy (COSY), **(e)** heteronuclear multiple-quantum correlation spectroscopy (HMQC), and **(f)** heteronuclear multiple-bond correlation spectroscopy (HMBC). The 1D and 2D nuclear magnetic resonance (NMR) spectroscopy results matched the properties of the ROCK2 inhibitor.

The experimental parameters are listed along with the individual spectra, where PULPROG is the pulse sequence, TD the size of the FID, NS the number of scan, SWH the spectral width, FIDRES the FID resolution, TE the temperature, and D1 the pre-scan delay. The length of the proton 90° pulse was 16 microseconds and that of 13C 10 microseconds. The spectrometer was a Bruker Avance III 500 MHz NMR system. DMSO-d6 was used as a solvent. To separate overlapping peaks in the 1-D 1H spectrum, that occasionally occur in 500 MHz NMR instruments, benzene-d6 was added drop-wise. Consequently, multiple 1-D and 2-D data sets were collected for structure determination.

a

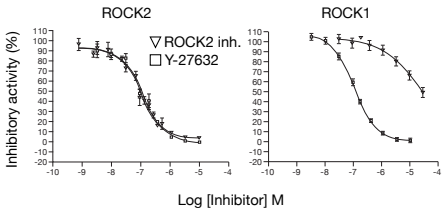

b

Ki (nM)	ROCK2 inh.	Y-27632	Fasudil
ROCK 2	41 ± 2	77 ± 5	112 ± 8
ROCK 1	> 10,000	68 ± 2	145 ± 7

c

Route	Dose (mg/kg)	C_{max} (ng/mL)	T_{max} (min)	$AUC_{0-tlast}$ (h*ng/mL)	$t_{1/2}$ (min)	Vz (L/kg)	CL (mL/min/kg)
iv	1	1620	<5	459	16	0.8	36
po	20	683	15	1359	68	14.8	1.7
po	60	3521	60	15208	253	55.2	2.3

d

Kinase	Activity (%)	IC_{50} (nM)
CK2 (h)	3	~100
Flt 3 (h)	24	5,100
MSSK1 (h)	27	>10,000
DRAK1 (h)	41	> 10,000
Ron (h)	44	>10,000
Fms (h)	46	>10,000
MuSK (h)	49	>10,000

Supplemental Figure 2, related to Figure 2: *Characterization of the ROCK2 inhibitor.* **(a)** The IC_{50} of the selective ROCK2 inhibitor and the dual ROCK1/2 inhibitor, Y-27632, for ROCK1 and ROCK2. The small molecule ROCK2 inhibitor selectively inhibited ROCK2 (IC_{50} ~105nM). In contrast to Y-27632 (IC_{50} 111nM), the ROCK2 inhibitor did not affect ROCK1 enzymatic activity at concentrations up to 10μM (IC_{50} 24μM). Briefly, recombinant ROCK1 and ROCK2 enzymes containing the truncated catalytic domains (PV3691 and PV3759) were purchased from Invitrogen and enzymatic activity was determined using [γ^{33}P]ATP (5μM) and S6 kinase substrate (17μM). The reaction was run for 45min at room temperature and was terminated by the addition of phosphoric acid. [γ^{33}P] phosphorylated S6 peptide was isolated by membrane filtration. The background was determined by running the reaction without enzyme. Radioactivity was assessed using a Microbeta Jet.

(b) Comparative enzyme inhibitor kinetics (Ki) of two existing dual ROCK1/2 inhibitors, fasudil and Y-27632 (Ishizaki et al., 2000), and the selective ROCK2 inhibitor. The selective ROCK2 inhibitor potently inhibits ROCK2, without affecting ROCK1. In comparison, Y-27632 and fasudil, showed equipotent inhibitory activities against ROCK1 and ROCK2. Therefore, in this study, the biological functions of the ROCK2 inhibitor were compared with the dual ROCK1/2 inhibitors fasudil and Y-27632.

IC_{50} was determined by curve fitting using GraphPad Prizm software (www.graphpad.com). The sigmoidal dose-response (variable slope) equation type analysis was used to generate the IC_{50} values. K_i values were calculated using the Cheng Prusoff equation of $K_i = IC_{50}/(1 + [S]/K_m)$, where [S] and K_m are the concentration of ATP and the K_m value of ATP, respectively (Lin et al., 1976).

Fasudil (HA-1077, 5-(1,4-diazepan-1-ylsulfonyl)isoquinoline hydrochloride, C14H17N3O2S.HCl, molecular weight 327.83) is in some countries an approved drug for the human use. In addition to ROCK, fasudil also inhibits, PKA, PKG, PKC, and MLCK with K_i values of 0.33μM, 1.6μM, 1.6μM, 3.3μM and 36μM, respectively.

(c) Pharmacokinetic parameters of the selective ROCK2 inhibitor. The inhibitor was administered orally (po) or intravenously (iv) at the indicated concentrations to mice and the pharmacokinetic parameters were calculated from the resulting time versus concentration curves by non-compartmental analysis using WinNonlin® (http://www.pharsight.com). T_{max}, time to reach C_{max}; C_{max}, the peak plasma concentration of the inhibitor after administration, AUC, area under the curve; $t_{1/2}$, elimination half time; Vz, volume of distribution; CL, clearance. C_{max}, $AUC_{0-tlast}$ and oral bioavailability (%F) of the ROCK2 inhibitor increased in a greater than dose responsive manner when the dose of the ROCK2 inhibitor was increased from 20mg/kg to 60mg/kg.

(d) The selectivity of the ROCK2 inhibitor was tested in the panel of over 220 representative enzymes from AGC, CMGC, TK, TKL, STE, CAMK, CK1 kinase families (KinaseProfiler™, Upstate Biology/Millipore). A small number of kinases were partially inhibited by the inhibitor at the measured 10μM concentration. IC_{50} measurements were performed for the kinases susceptible to inhibition by the ROCK2 inhibitor (IC_{50}Profiler™, Upstate Biology/Millipore). Detailed assay description, www.millipore.com/techpublications/tech1/pf3036. 'h', human,.

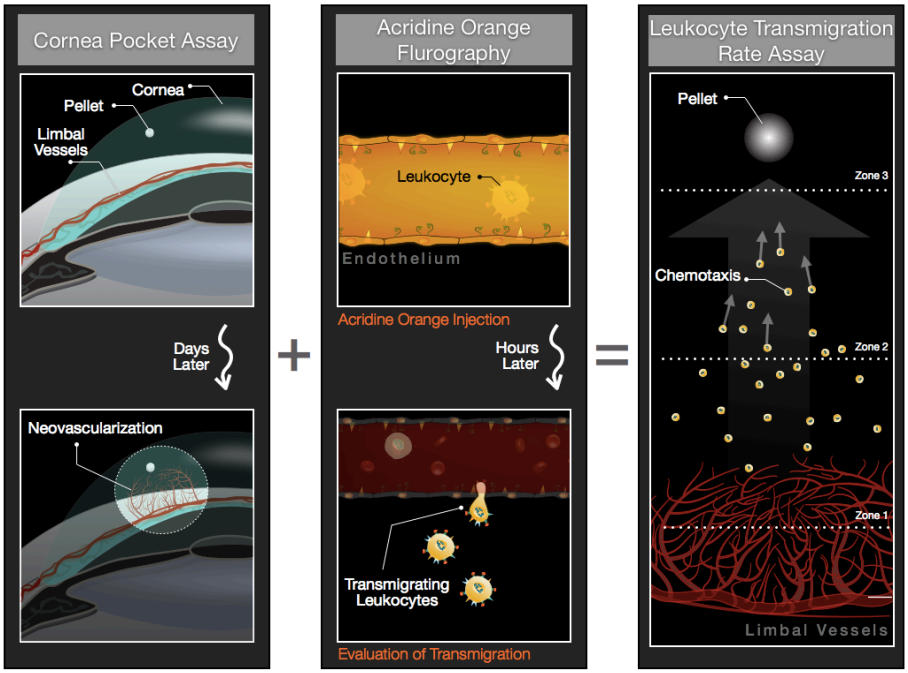

Supplemental Figure 3, related to Figure 4d: ***Model of leukocyte infiltration in the cornea.*** Schematic of our imaging technique for visualization of transmigrated leukocytes. By combining the growth factor-induced corneal angiogenesis with *in vivo* acridine orange labeling of leukocytes we developed a model, in which the leukocyte extravasation rate from limbal and angiogenic blood vessels is visualized and quantified.

Supplemental Experimental Procedure: Leukocyte transmigration assay

To visualize the leukocyte transmigration rate, we used our recently introduced assay (Nakao et al., 2012). Mice were anesthetized with ketamine (100mg/kg) and xylazine (10mg/kg). Poly-HEMA pellets (0.3µl, P3932; Sigma, St. Louis, MO, USA) containing 400ng MCP-1 (479-JE-010/CF, R&D systems) were prepared and implanted into the corneas. Cytokine pellets were positioned at ~0.8–1.0mm distance from the corneal limbus. After implantation, bacitracin ophthalmic ointment (E. Fougera & Co., Melville, NY, USA) was applied to each eye to prevent infection.

To stain the leukocytes, 500µl AO (1mg/ml) was injected intravenously. Two hours after AO injection blood vessels were stained by perfusing the animals with rhodamine-labeled concanavalin A lectin (ConA; Vector Laboratories, Burlingame, CA, USA), 10µg/ml in PBS (pH 7.4). Briefly, under deep anesthesia, the chest cavity was opened, and a 24-gauge perfusion needle was placed into the aorta. Drainage was achieved by opening the right atrium. The animals were then perfused with 10ml PBS to wash out blood cells in the vessels. After PBS perfusion, the animals were perfused with 5 ml rhodamine-labeled ConA and subsequently with 5ml PBS to remove residual unbound ConA. Immediately after perfusion, the corneas were carefully removed, and flatmounts were prepared using a mounting medium (TA-030-FM, Mountant Permafluor; Lab Vision).

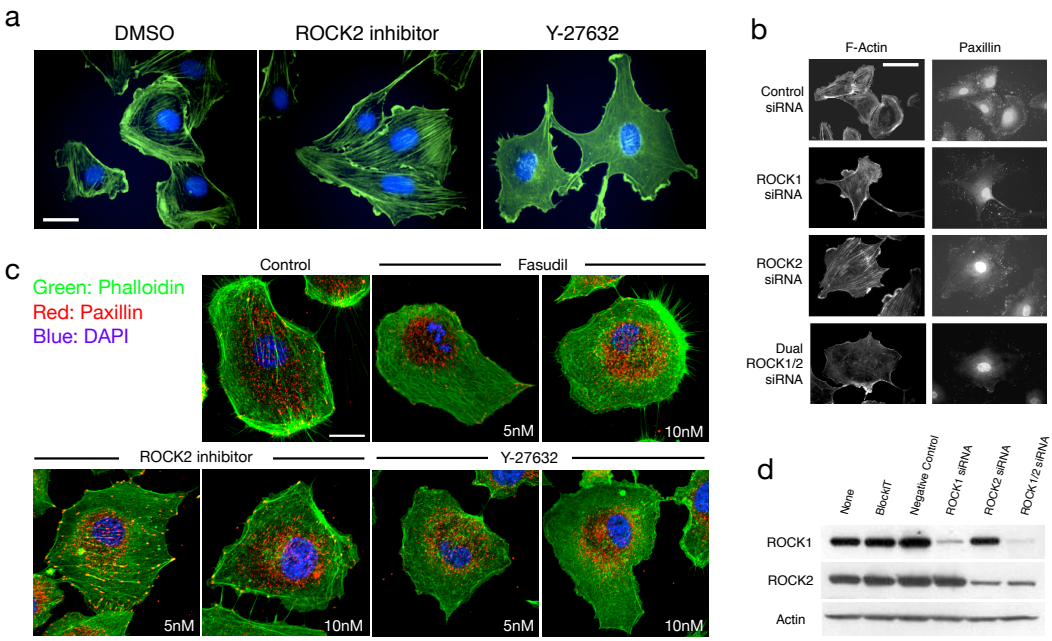

Supplemental Figure 4, related to Figure 4: ***Impact of ROCK inhibition on cytoskletal structures*****. (a)** Cytoskeletal structures of HUVECs treated with the ROCK2 inhibitor or Y-27632 at 10μM for four hours under normal culture condition. The cells were stained for actin (*green*) and nucleus (*blue*) using phalloidin and DAPI, respectively. ROCK2 inhibition does not affect the characteristic cytoskeletal structure, while dual ROCK1/2 inhibition with Y-27632 resulted in an atypically uniform cytoskeletal staining. Scale bar, 20μm. **(b)** HUVEC cells were stained for the cytoskeletal proteins F-actin and paxillin. ROCK1 blockade diminishes but ROCK2 blockade does not affect cytoskeletal structures. Scale bar, 20μm. **(c)** The effect of dual ROCK1/2 or ROCK2 inhibition on paxillin distribution was examined in cultured endothelial cells that were inhibitor treated for 30min at two different concentrations. These cells were stained for phalloidin and paxillin. In the vehicle treated controls, paxillin was distributed in the cytoplasm. When both ROCK isoforms were blocked, using the dual ROCK1/2 inhibitors fasudil or Y-27632, paxillin was no longer found evenly spread in the cytoplasm. In these cells paxillin was concentrated in the nuclear or immediate perinuclear regions. In comparison, in the ROCK2 inhibitor treated cells, paxillin distribution in the cells was comparable to the control cells. These results confirm the impact of ROCK isoform knockdowns with siRNAs. More in-depth studies of the cytoskletal changes will be required to understand the individual roles of ROCK isoforms in paxillin signaling and focal adhesion kinases. Scale bar, 20μm. **(d)** Western analysis of HUVECs transfected with siRNA targeting of ROCK1, ROCK2, or both. Negative control, a scramble 20-mer RNA. BlockIt (Invitrogen), a fluorescently labeled RNA to track uptake/transfection efficiency.

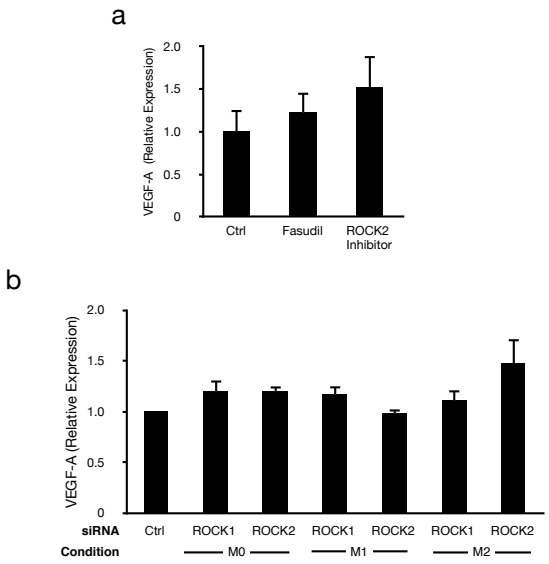

Supplemental Figure 5, related to Figure 6: ***ROCK signaling in macrophages does not affect VEGF-A expression*****.** VEGF-A is an important growth factor in AMD pathology. VEGF-A inhibition is the current standard in AMD treatment. To examine the role of ROCK signaling in VEGF-A secretion in macrophages, we measured this growth factor in cultured RAW 264.7 monocytes that were in M0, M1, and M2 state of differentiation. **(a)** Neither pharmacologic nor **(b)** gene blockade of ROCK isoforms affected VEGF-A gene or protein expression in M0, M1, or M2 macrophages. These data indicate that the anti-angiogenic and anti-leakage properties of ROCK inhibition is unrelated to VEGF-A secretion from macrophages. In line with this finding, our recent clinical data showed that ROCK inhibition ameliorates anti-VEGF resistant diabetic macular edema (DME) (Ahmadieh et al., 2013; Nourinia et al., 2013).

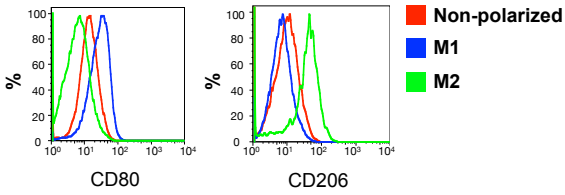

Supplemental Figure 6, related to Figure 7a: *Macrophage polarization*. For quality control, the M1 and M2 differentiated bone marrow derived macrophages were characterized by flow cytometry.

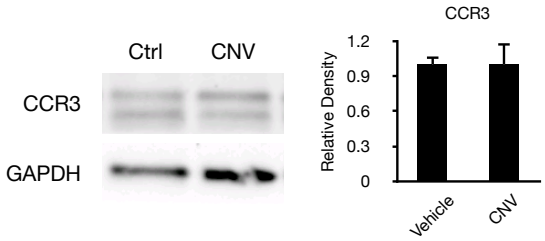

Supplemental Figure 7, related to Figure 5b & 7e: *CCR3 expression unchanged in laser-induced CNV*. CCR3 is a chemokine receptor involved in eosinophil and basophil trafficking. CCR3 is also found in TH2 cells (Sallusto et al., 1997) and is thought to take part in the type 2 response (Mantovani et al., 2004). Monocytes express CCR3, albeit at lower levels. CCR3 was reported to be elevated in CNV lesions in human AMD without any involvement of inflammation (Takeda et al., 2009). Surprisingly, our results did not show a difference in CCR3 protein expression in CNV compared to unlasered normal controls. Representative western blot from mouse choroidal tissues with and without laser injury. *n*=3 animals in each group.

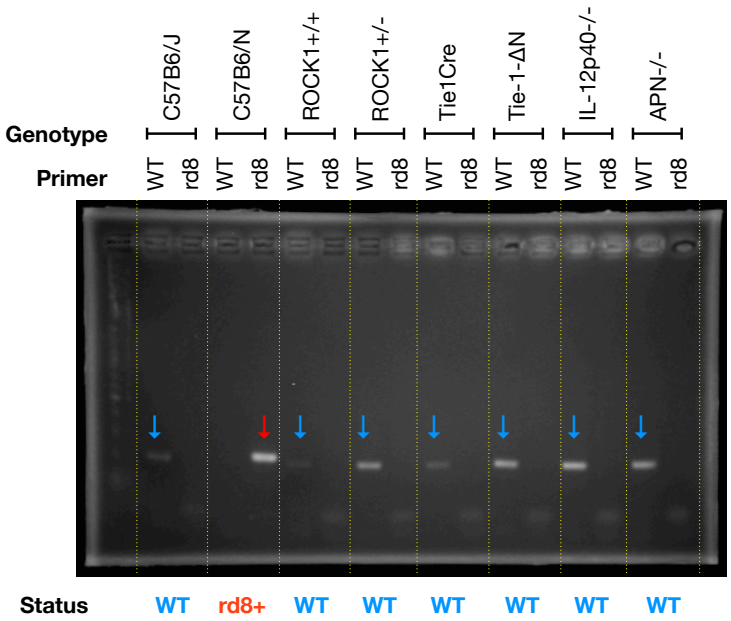

Supplemental Figure 8, related to Materials and Methods: ***Testing for the rd8 in the Crb1 gene.*** The rd8 mutation in the Crb1 gene causes retinal degeneration and AMD like features, which was previously erroneously attributed to other causes (Luhmann et al., 2013), i.e. deficiency of the Ccl2/Cx3cr1 genes (Ambati et al., 2003). Several vendor lines are contaminated with the rd8 mutation (Mattapallil et al., 2012), which made it necessary to inspect for the mutation in our experimental lines for quality control. For this purpose the PCR method, described by (Mehalow et al., 2003), was used. Representative results for each strain in our study is shown, where the size of the WT allele is 220 bp and the rd8 allele 244 bp. The results show that the mice used in our study were WT for the Crb1 gene.

Supplemental Experimental Procedure: Detection of the rd8 mutation by PCR

A fully automated nucleic acid extractor (Magtration System 6GC, PSS Co., Chiba, Japan) with a Magtration Genomic DNA Purification Kit (PSS Co.) was used to extract and purify the genomic DNA of mouse tail biopsy samples. DNA samples isolated from tail biopsies were amplified separately for wild type (WT) allele and mutant rd8 allele using primers specified by (Mehalow et al., 2003). Primer sequences included mCrb1 mF1: GTGAAGACAGCTACAGTTCTGATC; mCrb1 mF2: GCCCCTGTTTGCATGGAGGAAACTTGGAAGACAGCTACAGTTCTTCTG; and mCrb1 mR: GCCCCATTTGCACACTGATGAC. The total volume in the individual PCR assays was 40 µl, including 0.5 µl template DNA, 1.0 µl (10µM) each of forward and reverse primer for WT allele, and 1.0 µl (10µM) forward and 0.5 µl (10µM) reverse primer for rd8 mutant allele and 0.2 µl of BIOTAQTM HS DNA polymerase (BIOLINE), and 20 µl of 2×Ampdirect® Plus (Shimadzu Corp, Kyoto, Japan) containing MgCl2 (3mM) and dNTPs (400µM each). Reactions initially were denatured at 94°C for 5 minutes followed by 35 cycles at 94°C for 30 seconds, 65°C for 30 seconds, 72°C for 30 seconds and a final extension at 72°C for 7 minutes. Amplicons were separated using 3% agarose gel and visualized under UV light after staining with ethidiumbromide. Amplicon sizes are WT allele=220 bp and rd8 allele=244 bp.

Supplemental References

Ahmadieh, H., Nourinia, R., and Hafezi-Moghadam, A. (2013). Intravitreal fasudil combined with bevacizumab for persistent diabetic macular edema: a novel treatment. JAMA Ophthalmol *131*, 923-924.

Ambati, J., Anand, A., Fernandez, S., Sakurai, E., Lynn, B.C., Kuziel, W.A., Rollins, B.J., and Ambati, B.K. (2003). An animal model of age-related macular degeneration in senescent Ccl-2- or Ccr-2-deficient mice. Nat Med *9*, 1390-1397.

Ishizaki, T., Uehata, M., Tamechika, I., Keel, J., Nonomura, K., Maekawa, M., and Narumiya, S. (2000). Pharmacological properties of Y-27632, a specific inhibitor of rho-associated kinases. Mol Pharmacol *57*, 976-983.

Lin, T.S., Neenan, J.P., Cheng, Y.C., and Prusoff, W.H. (1976). Synthesis and antiviral activity of 5- and 5'-substituted thymidine analogs. J Med Chem *19*, 495-498.

Luhmann, U.F., Carvalho, L.S., Robbie, S.J., Cowing, J.A., Duran, Y., Munro, P.M., Bainbridge, J.W., and Ali, R.R. (2013). Ccl2, Cx3cr1 and Ccl2/Cx3cr1 chemokine deficiencies are not sufficient to cause age-related retinal degeneration. Exp Eye Res *107*, 80-87.

Mantovani, A., Sica, A., Sozzani, S., Allavena, P., Vecchi, A., and Locati, M. (2004). The chemokine system in diverse forms of macrophage activation and polarization. Trends Immunol *25*, 677-686.

Mattapallil, M.J., Wawrousek, E.F., Chan, C.C., Zhao, H., Roychoudhury, J., Ferguson, T.A., and Caspi, R.R. (2012). The Rd8 mutation of the Crb1 gene is present in vendor lines of C57BL/6N mice and embryonic stem cells, and confounds ocular induced mutant phenotypes. Invest Ophthalmol Vis Sci *53*, 2921-2927.

Mehalow, A.K., Kameya, S., Smith, R.S., Hawes, N.L., Denegre, J.M., Young, J.A., Bechtold, L., Haider, N.B., Tepass, U., Heckenlively, J.R*., et al.* (2003). CRB1 is essential for external limiting membrane integrity and photoreceptor morphogenesis in the mammalian retina. Hum Mol Genet *12*, 2179-2189.

Nakao, S., Zandi, S., Faez, S., Kohno, R., and Hafezi-Moghadam, A. (2012). Discontinuous LYVE-1 expression in corneal limbal lymphatics: dual function as microvalves and immunological hot spots. FASEB J *26*, 808-817.

Nourinia, R., Ahmadieh, H., Shahheidari, M.H., Zandi, S., Nakao, S., and Hafezi-Moghadam, A. (2013). Intravitreal fasudil combined with bevacizumab for treatment of refractory diabetic macular edema; a pilot study. J Ophthalmic Vis Res *8*, 337-340.

Sallusto, F., Mackay, C.R., and Lanzavecchia, A. (1997). Selective expression of the eotaxin receptor CCR3 by human T helper 2 cells. Science *277*, 2005-2007.

Sweetnam, P., Bartolozzi, A., Campbell, A., Cole, B., Foudoulakis, H., Kirk, B., Seshadri, H., and Ram, S. (2010). Rho kinase inhibitors. WO2010104851 A1.

Takeda, A., Baffi, J.Z., Kleinman, M.E., Cho, W.G., Nozaki, M., Yamada, K., Kaneko, H., Albuquerque, R.J., Dridi, S., Saito, K*., et al.* (2009). CCR3 is a target for age-related macular degeneration diagnosis and therapy. Nature *460*, 225-230.